DEVELOPMENT OF EMBEDDED SENSORS FOR STRUCTURAL HEALTH MONITIROING OF WIND TURBINE BLADES

by

Edward Charles Meehan

A thesis submitted in partial fulfillment
of the requirements for the degree

of

Master of Science

in

Mechanical Engineering

MONTANA STATE UNIVERSITY
Bozeman, Montana

November 2012

APPROVAL

of a thesis submitted by

Edward Charles Meehan

This thesis has been read by each member of the thesis committee and has been found to be satisfactory regarding content, English usage, format, citation, bibliographic style, and consistency and is ready for submission to The Graduate School.

Dr. Douglas Cairns

Approved for the Department of Mechanical Engineering

Dr. Christopher H. M. Jenkins

Approved for The Graduate School

Dr. Ronald W. Larsen

STATEMENT OF PERMISSION TO USE

In presenting this thesis in partial fulfillment of the requirements for a master's degree at Montana State University, I agree that the Library shall make it available to borrowers under rules of the Library.

If I have indicated my intention to copyright this thesis by including a copyright notice page, copying is allowable only for scholarly purposes, consistent with "fair use" as prescribed in the U.S. Copyright Law. Requests for permission for extended quotation from or reproduction of this thesis in whole or in parts may be granted only by the copyright holder.

Edward Charles Meehan

November 2012

ACKNOWLEDGMENTS

I would like to acknowledge everyone who provided insight and assistance in the work presented in this report. Primarily, I would like to thank Dr. Cairns for his guidance during the progression of this project. I would also like to thank Sandia National Laboratories and Joshua Paquette for their funding and input. Thanks to the entire composites group, who helped with the manufacturing of composite plates, especially Tiok Agastra and Patrick Flaherty for teaching me the tricks to making a consistent plate. Finally I would like to thank all of my friends and family who supported me throughout my graduate work.

TABLE OF CONTENTS

TABLE OF CONTENTS - CONTINUED

LIST OF TABLES

LIST OF FIGURES

Figure Page

LIST OF FIGURES - CONTINUED

Figure Page

LIST OF FIGURES - CONTINUED

Figure Page

LIST OF FIGURES - CONTINUED

Figure Page

ABSTRACT

Monitoring a structure's response to various loading conditions is essential to being able to predict catastrophic failure of the part. There are many types of sensors that have been developed to be able to accurately measure these important quantities. However, as the structure becomes thicker, it is important to monitor in more places than just the surface of the material. Composite materials, such as those used in the wind turbine industry, are typically built in layers, which lend themselves to having sensors embedded in the structure. Previous research had focused on how these embedded sensors affected the mechanical properties of the material, and this research continues on by utilizing the gages to monitor the strains developed in the material. An important aspect of the research was to be able to separate the mechanical strain from the thermal strains developed in the substrate. This was achieved by using advanced circuitry, and was confirmed by performing tensile and heating tests on both surface mounted and embedded sensors. From the data collected, it was shown that it was possible to separate out the mechanical and thermal strains.

INTRODUCTION

As the demand for energy is constantly increasing and the availability of non-renewable sources of energy is constantly being depleted, the need for various forms of green or renewable energy sources is becoming more and more important. Solar, geothermal, hydro, and wind are just a few of the sources of energy that are being harnessed and implemented today.

Composite materials have been instrumental in allowing wind energy to become a practical form of energy generation. They allowed a massive increase in the size of blades due to the ability to decrease the weight to stiffness ratio in response to the ability to tailor material properties in specific directions [1]. However, the cost of composite materials is typically more expensive than standard engineering materials such as aluminum and steel. So to make the composite blades cost effective, the quality of materials and manufacturing is much lower than that in the aerospace field. This leads to a material that is more prone to failure than would be expected for a pristine sample of a similar composite material.

In an effort to maximize the output of each turbine, the size of the blades continues to increase. This increase in size amplifies the stresses in the components due to increased gravitational and rotational effects. In Germany, the world's largest wind turbine to date has been installed, and is estimated to produce 7+ megawatts, and has a rotor diameter of 126 meters. A standard 40 meter blade (for a 1.5 MW turbine) will weigh 6 to 7 tons, so the gravitational forces experienced by these large blades are

immense [2]. This turbine is shown in Figure 1 and has recently been installed in Germany.

Figure 1. The world's current largest wind turbine: Enercon E-126 [3]

Composite materials fail in ways different from their metallic counterparts. Due to this property, when damage occurs in the component, it can become catastrophic very quickly. One way of finding the damage is through non-destructive testing (NDT). This usually requires running an ultrasonic transducer over the surface of the blade, and comparing it to the known profile of the thickness, which is a time intensive process. GE has recently developed a robot to climb over the surface of the tower and blades in order to reduce some of the inspection time from human labor [4]. Currently, it is only

mounted with a camera in order to locate any surface flaws. However, they are now looking at installing a microwave scanner so as to look inside the material for any spots of delamination or other defects. In Figure 2, the robot is climbing the side of a tower using its vacuum pump to keep it firmly against the surface.

Figure 2. GE's remote-controlled wall climbing robot used to photograph the blades and look for failure points

Surface mounted sensors have found their way into monitoring the stresses and strains of many different materials. When these sensors are exposed to the environment, they often degrade quickly as compared to a laboratory environment. The rain, humidity, ice, and any other weather phenomena can greatly damage the sensors. Also, the stresses and strains can vary greatly through the thickness of the sample, so the surface strains are not always indicative of what is happening at the midpoint of the sample. This has led to

interest in embedding sensors between the lamina of the composite material, as the manufacturing process of composites allows for this step to be implemented.

A previous master's thesis dealt with the experimental strength decrease due to embedded sensors in a composite material. Several strength tests were performed and compared to virgin samples to quantify this value. Chemical treatment of the sensors was also investigated so as to have the best adhesion to the matrix material in the composite and give the best mechanical properties.

After proving that the diminished properties were not detrimental to the overall structure, the next step was to take measurements from these sensors, and prove their ability to be used in the structural health monitoring of the wind turbine blades. One of the primary goals was to measure both strain and temperature from a set of similar sensors. This could be accomplished using some modified circuitry. Several experiments involving tension tests and/or heating were performed to validate the hypothesis.

BACKGROUND

Wind Energy

History

The desire to use the wind as a tool to create a mechanical force goes back several centuries. Harnessing the wind was first recorded by the Persians in roughly 900 AD using a vertical axis style windmill [5]. However, the most recognizable examples of windmills are the Dutch Windmills that started to show up in the 1600s. These had a horizontal axis and therefore, look much more like the wind turbines we see today. The primary purpose of these windmills was to pump water or grind grain [6].

Figure 3. The Lily Windmill, a Dutch style windmill [7]

These systems lost much of their popularity because the wind could not be stored and used when needed, and they were a stationary system [5]. The interest in wind energy really started back up in the 1960s when people started to realize the consequences of using fossil fuels so extensively. As seen in Figure 4, the trend to harness more energy from a single turbine has led to larger structures, which place a higher demand on the materials used.

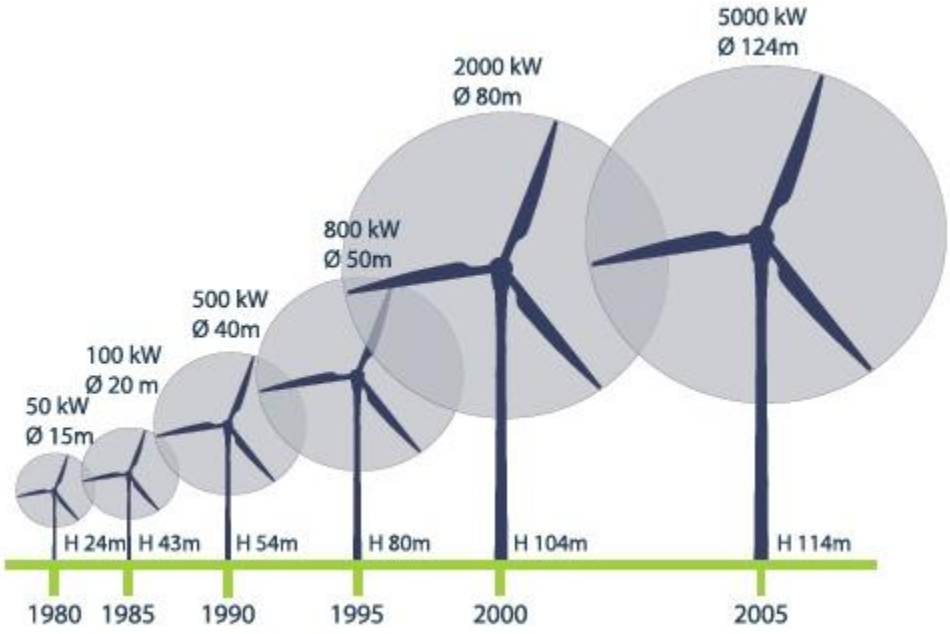

Figure 4. Trend in wind turbine size

The typical size of the wind turbines that are installed on land are of the 1.5 megawatt variety, as seen in the Judith Gap Wind Farm shown in Figure 5. With a total of 90 turbines, it is estimated to produce 150 megawatts [8]. The larger turbines that are being developed are typically planned for off shore usage.

Figure 5. The Judith Gap Wind Farm in Montana

Wind Turbine Structure

Wind turbine structures contain three primary features; the blades, the nacelle, and the tower. The tower's main purpose is to support the weight of the nacelle and blades. It also provides an access point for getting to the components in the nacelle. The nacelle contains all of the components to transfer the rotation of the blades, into electricity. The blades, which will be discussed in more detail, are the most important part of a wind turbine, as they transfer a horizontal fluid flow (wind) into a rotational force that can be turned into electricity. The way in which all of the components fit together is illustrated in Figure 6.

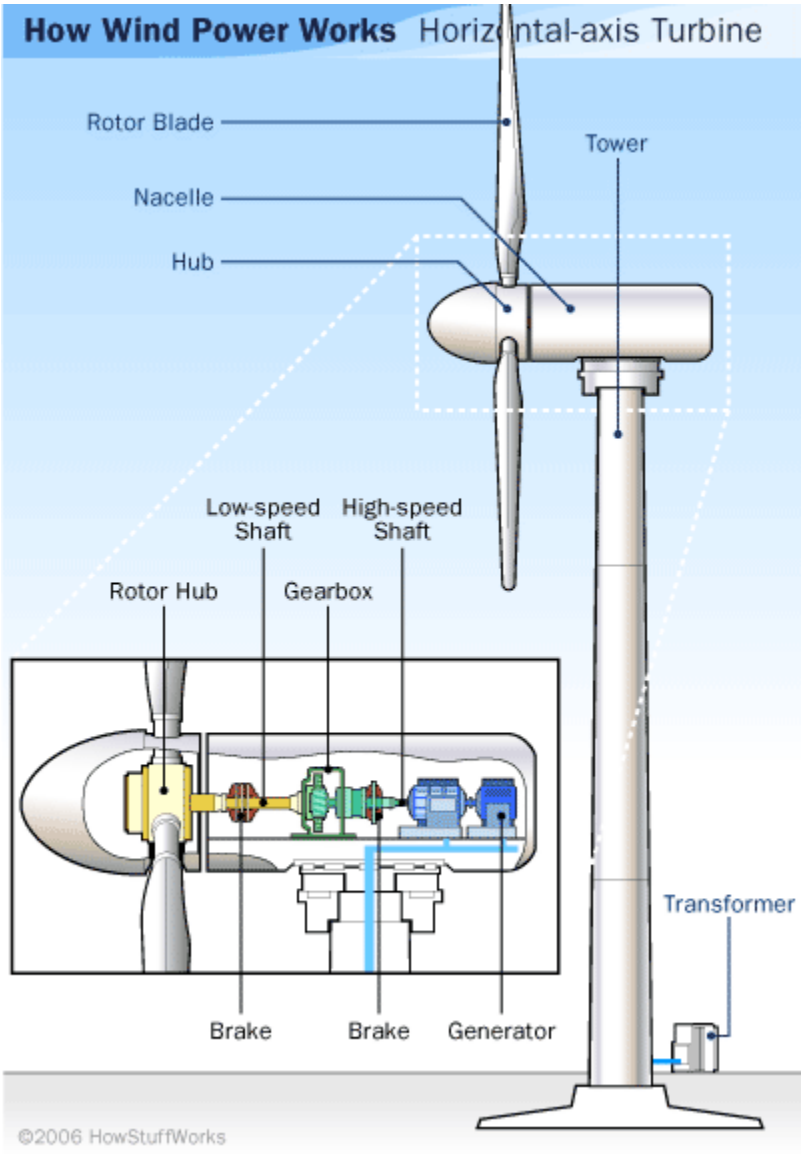

Figure 6. Structural components of a wind turbine

Blade Design & Manufacturing

As with any other structure, the wind turbine blade is designed according to the loads that are expected to be seen. The most prominent load is the flapwise bending due to the lift forces. This load is handled mostly by the spar cap and shear webs [9]. A

major portion of the design is spent balancing the aerodynamic efficiency and the structural efficiency through an iterative approach.

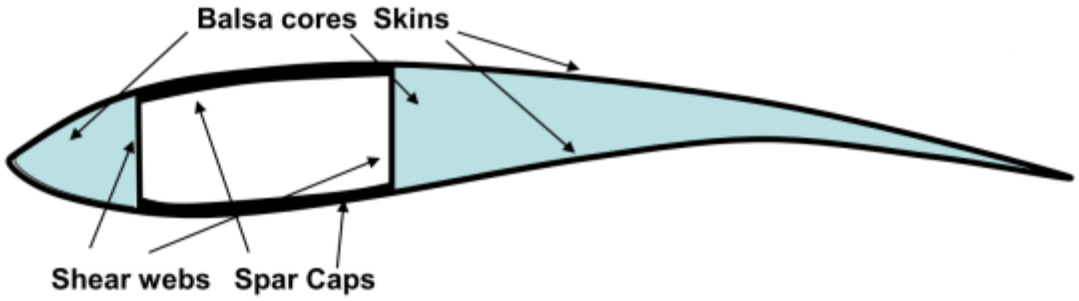

Figure 7. Typical cross sectional view of a wind turbine blade

As described in Figure 8, there are several loading conditions to take into consideration while designing a wind turbine. But as many of these are stoichiometric, it is difficult to build to a certain stress level. The other factor that needs to be considered when designing these blades is the cost.

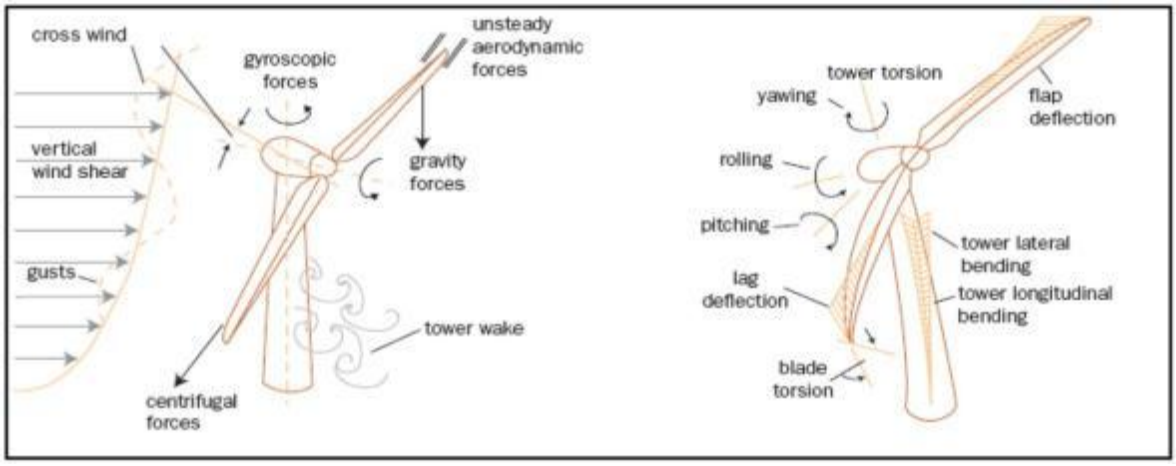

Figure 8. The loading conditions that a wind turbine will typically undergo

Future of Wind Energy

As was mentioned in the introduction, some of the wind turbines are now capable of producing 7+ megawatts. Since these are physically larger than the 1.5 megawatt turbines, they also can withstand stronger winds, and require these winds to be efficient. Therefore, offshore wind farms have become more popular with the increase in the build and design quality of the larger blades. One of these offshore farms is shown in Figure 9. These offshore farms seem to be the current trend, as the offshore winds are typically stronger and more consistent than those on land. Many large cities are typically built around a harbor or near the ocean [10], so this potential energy source is close to these cities, but often untapped.

Figure 9. An offshore wind farm in Arklow Bank, Ireland [10]

These offshore farms have huge potential for generating electricity. At the Dogger Bank Offshore Wind Farm in the UK, which is currently under development, it is estimated that it could provide 13000 megawatts of electricity if fully developed. When compared to the 150 megawatts that the Judith Gap Wind Farm is producing, the potential energy from these offshore farms is huge [11].

Composite Materials

Basics

A composite material is formed by combining two or more distinct materials. Wood is the most common example found in nature, and it is made of cellulose fibers in a lignin matrix. Typical manmade composites are composed of a fibrous or particulate component held together in a matrix material. Manmade composites have become instrumental in forwarding the aerospace field, since it is possible to tailor the material in a particular direction, which allows them to achieve higher stiffness to weight ratios than with other materials. Predicting mechanical properties of composite materials can become quite complex due to the non-isotropic nature of composite materials [1]. Since only uni-directional composite samples were tested for this research, the simplest composite analytical model can be used. This model is the rule-of-mixtures, and is shown in Equation 1, and is used to predict the modulus of elasticity of a continuous fiber material along the fiber principal direction.

$$E_1 = E_m + V_f(E_f - E_m) \qquad \text{Equation 1}$$

Where

$E_1 = Modulus\ of\ composite\ in\ fiber\ direction$
$E_m = modulus\ of\ matrix\ material$
$E_f = modulus\ of\ fiber\ material$
$V_f = volume\ fraction\ of\ fiber$

To compute the strain in the material, Hooke's law for a transversely isotropic material can be used since there is no coupling between the curvature and normal loads due to the balanced and symmetric nature of the laminate. From Equation 2, it can be shown that with no stress in the 2 direction (perpendicular to the fiber direction), the strain in the fiber direction can be simplified to $\epsilon_1 = \frac{\sigma_1}{E_1}$.

$$\begin{Bmatrix}\epsilon_1\\ \epsilon_2\\ \epsilon_6\end{Bmatrix} = \begin{bmatrix} \frac{1}{E_1} & -\frac{\nu_{21}}{E_2} & 0 \\ -\frac{\nu_{12}}{E_1} & \frac{1}{E_2} & 0 \\ 0 & 0 & \frac{1}{G_{12}} \end{bmatrix} \begin{Bmatrix}\sigma_1\\ \sigma_2\\ \sigma_6\end{Bmatrix} \qquad \text{Equation 2}$$

Where

$\epsilon_i = material\ strain\ in\ the\ i\ direction$
$\sigma_i = material\ stress\ in\ the\ i\ direction$
$\nu_i = Poisson's\ ratio\ in\ the\ i\ direction$

It is a well-known fact that composite materials are usually much more expensive per pound than most other engineering materials. This is not necessarily due to limited resources, but rather the labor required in lying the parts up. Although laying the higher quality parts up is now becoming automated, many companies still layup by hand, but require meticulous workers to ensure that there are no wrinkles or obvious manufacturing defects. However, when manufacturing very large structures, such as wind turbine

blades, it is much harder to find a single wrinkle in the material, and as shown in Figure 10, the inspectors will often walk on top of the blade to look for flaws, which can likely induce more flaws into the material.

Figure 10. Hand layup of composite wind turbine blade [12]

Failure Methods

The nature of composite materials leads to many more complex and varied failure methods when compared to a typical metallic material. Some of the major failure modes are shown in Table 1. These various methods of failure make strength predictions of composite materials much more difficult.

Table 1. Description of different types of composite failures

Type of Failure	Description
Delamination	Separation of lamina
Fiber Debonding	Bond between the fiber and matrix fails
Fiber Breaking	Tensile failure of just the fiber
Matrix Crazing	Micro-crack formation in the matrix
Matrix Cracking	Larger cracks form in the matrix

Since each combination of fiber and matrix will have different properties, the standard for determining the failure criteria is through extensive testing of the samples. This has led to several failure criteria for laminates that can be used for failure prediction. The tests typically used for this are shown in Figure 11, and typically tensile, compressive, or shear tests to failure.

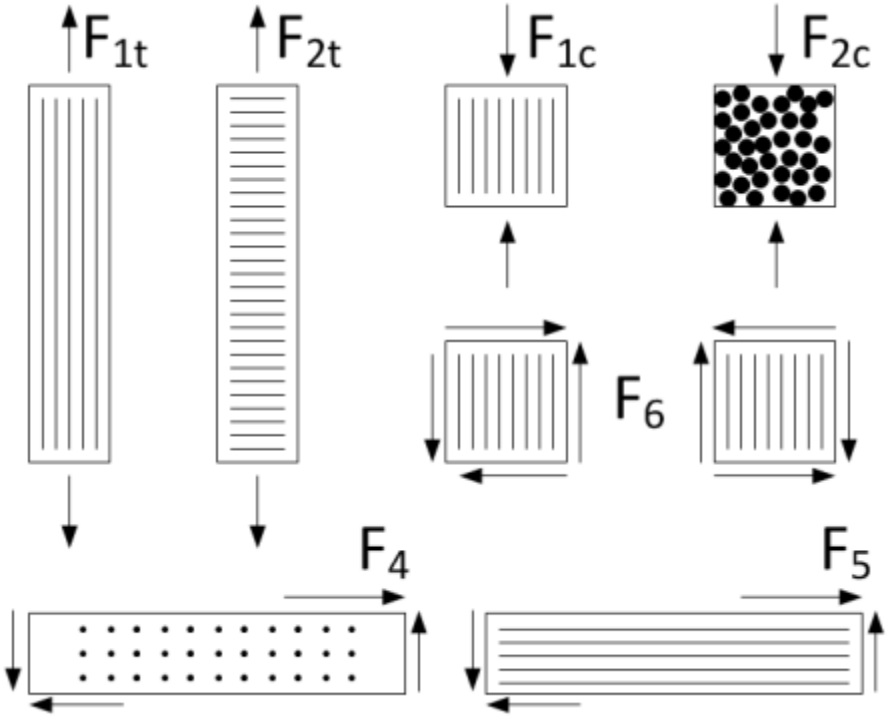

Figure 11. Failure testing performed to develop failure criteria

Sensors

A sensor is defined as ‘a device that responds to a physical stimulus (such as heat, light, sound, pressure, magnetism, or a particular motion) and transmits a resulting impulse (as for measurement or operating a control)’ [13]. Sensors are essential to

monitoring a structure, as they allow the user to quantitatively, rather than qualitatively analyze a system.

Sensors are typically attached to the surface of the sample being measured using an adhesive. Surface measurements can be very useful, but they don't always represent what is happening inside of the material. However, not all materials lend themselves to having sensors embedded in them. It can be quite difficult to install a sensor inside a block of aluminum. Composite structures and some polymers simplify the process, as the liquid polymer or resin can cure around the sensor, completely encapsulating the sensor inside of the material.

Previous Embedded Sensor Research

The embedded sensor work began with the desire to develop adaptive blades that could alter their shape or position to the current wind load, thus becoming more efficient. One of the methods to determine the most optimum shape or position is by sensing the strain in certain locations in the blade, and adjusting accordingly [14].

A gurney style flap, which is designed to increase the lift on an airfoil, was designed to react to the loads determined by the sensors, so as to shed the wind loads from the blade. Several prototypes (Figure 12) were manufactured that embodied this concept; however it was not the response from embedded sensors that signaled the actuation of the flap.

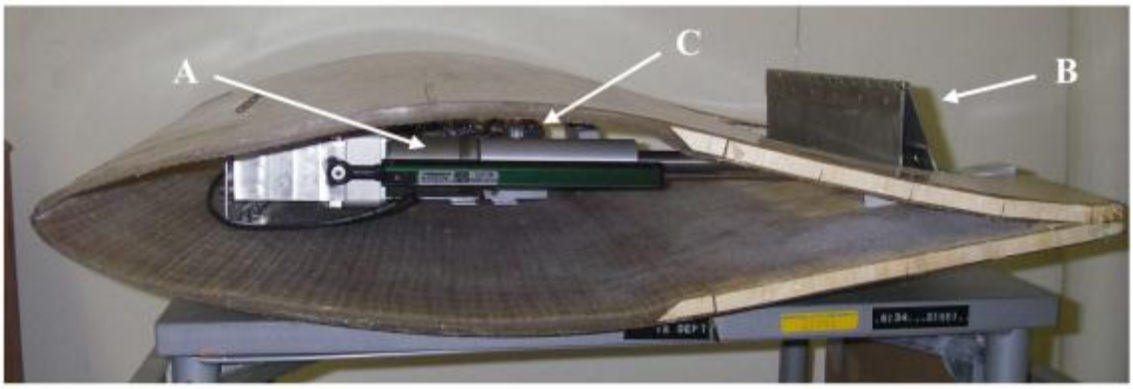

Figure 12. Gurney Flap prototype with labeled components: A) Linear actuator, B) Gurney flap, and C) Relay assembly

Nathan Palmer's research [15] focused in on the actual senor embedment. Several sensors were investigated for their practicality in use with the turbine blades. Metal foil strain gages, PVDF film, and Fiber Optics were all embedded and tested. This research focused on the mechanical effects that the sensors had on the material. By performing several tensile and mode 1 fracture tests, the properties of the composite with embedded sensors were compared to those of the virgin samples.

Multiple methods of treating the sensors were employed to determine which method was the least harmful to the mechanical properties of the composite sample. The failure strength of the composite with two different matrix materials, and 3 different sensor treatments is displayed in Figure 13. Similar tests were performed for the tensile modulus, and repeated for the PVDF films and fiber optic cable.

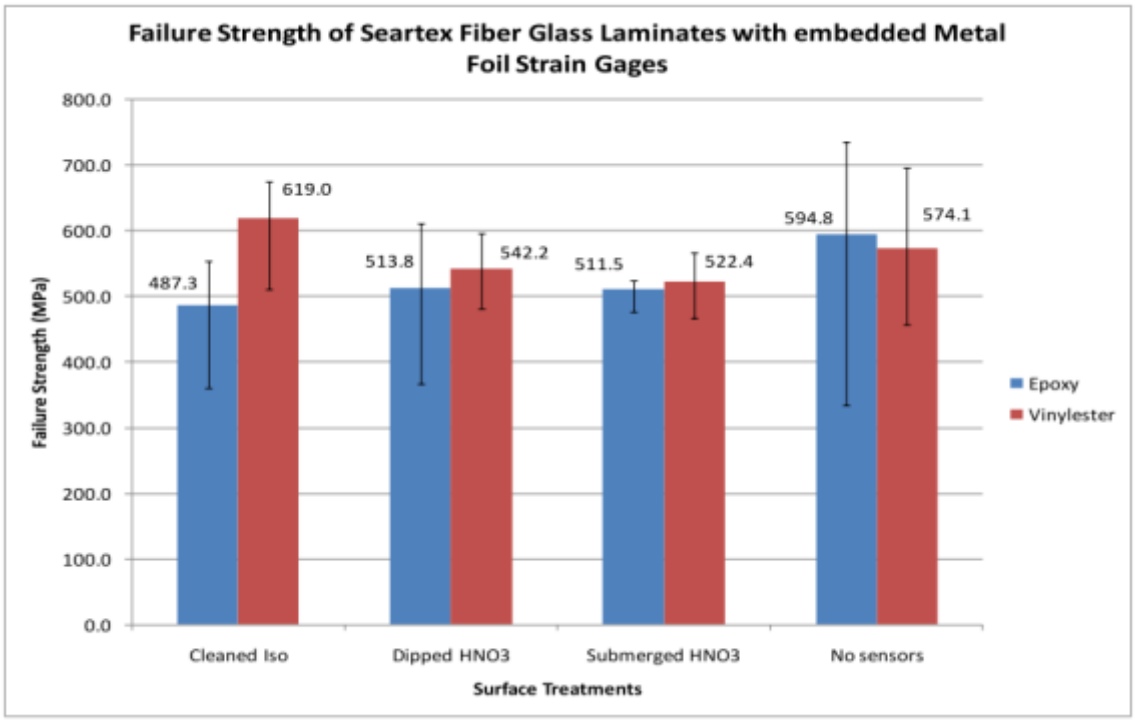

Figure 13. Strength trends of the embedded strain gages

Field Emission Scanning Electron Microscopy (FESEM) images were taken to investigate the bonding between the sensor and the matrix material. It was a result of this testing that the sensor treatment was investigated. A cross section of a MFSG embedded in a composite sample is represented in Figure 14. It is clear that the resin was not adhering well to the gage when no treatment was applied.

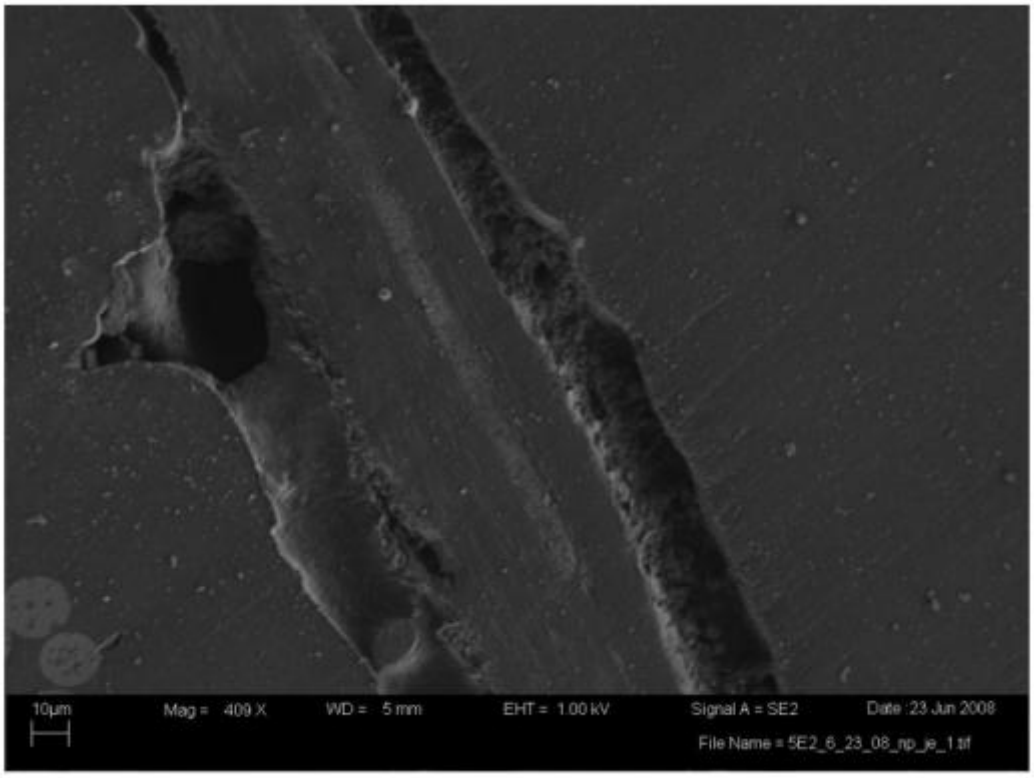

Figure 14. FESEM image of cross section of embedded strain gage.

From all of the testing performed, it was determined that the best treatment for the sensors was to submerge it in a 20% by weight Nitric acid solution for ten seconds, and then clean it with Isopropyl Alcohol.

Since the sensors are being embedded during the manufacturing process, the resin needs to cure around the sensor. The curing process is very important to ensure the quality of the composite material. Several sensors can be used to monitor the curing process such as dielectric sensors, but it would be desirable to use the embedded sensors that will be used for structural health monitoring as cure monitoring gages. This is the basis for a concurrent thesis that has gone hand-in-hand with the research presented in this thesis.

Testing Plan

In order to prove that the selected sensors could be successfully embedded and utilized in a composite material, the following test plans were developed and followed. In Table 2, the experiments performed to characterize the metal foil strain gages are listed in the order they were performed, along with the reason for performing the experiment. The tensile testing was performed first as it was most predictable. Once the heating tests were finished, the combined loading experiment was performed. Typically, the tests were repeated two times to ensure that the results obtained were due to the applied loading condition, and not just some anomalous result. It was also important to ensure that the results were consistent with one another, showing the same sensitivity to similar loading. The testing on the aluminum bars was usually only repeated once, since it was simply a test to ensure that the circuit was working correctly. A similar test plan for the PVDF films is outlined in Table 3. A combined loading scenario was not performed due to the quick decay of the response.

Table 2. Testing plan for metal foil strain gages

	Experiment	Purpose	# of tests performed
Tensile	Instron test of gages adhered to aluminum bar	Ensure gages are working properly	2
	Instron test of gages adhered to surface of composite sample	Have a baseline sample to compare to embedded gages	3
	Tensile test of composite sample with embedded gages	Collect data from an embedded sensor	3
	Tensile test of composite sample with embedded gages along with extensometer	Correlate the data obtained from the sensor to an accurate external measurement	3
Heating	Controlled heating of gages adhered to aluminum bar	Make sure the heating is effecting the gages as expected	2
	Controlled heating of gages adhered to surface of composite sample	Ensure that the lower CTE does not affect the response too drastically	3
	Controlled heating of embedded gages	Eliminate the immediate effects of the ambient conditions on the gages	3
Combined	Controlled heating and tensile loading of embedded gages	Separate the mechanical and apparent thermal strains	3

Table 3. Testing plan for PVDF film

	Experiment	Purpose	# of tests performed
Tensile	Tensile test of gages with different time constant parameters	Investigate the effects of varying the capacitance and resistance with respect to the magnitude and decay profile of the response	2
	Instron test of gages adhered to aluminum bar	Ensure gages are working properly	3
	Instron test of gages adhered to surface of composite sample	Have a baseline sample to compare to embedded gages	3
	Tensile test of composite sample with embedded gages	Collect data from an embedded sensor	3
	Tensile test of gages adhered to aluminum bar (varying load rates)	Show that the sensors are more suited for sensing the magnitude of a transient event	3
Heating	Controlled heating of gages adhered to aluminum bar	Make sure the heating is effecting the gages as expected	2
	Controlled heating of gages adhered to surface of composite sample	Ensure that the lower CTE does not affect the response to drastically	3
	Controlled heating of dual configuration circuit	Prove that the pyroelectric response can be canceled out	3

To resolve many of the straight forward issues when testing the sensors, a basic logic table was developed to guide the user through some of the main troubleshooting solutions. This logic table is shown in Figure 15.

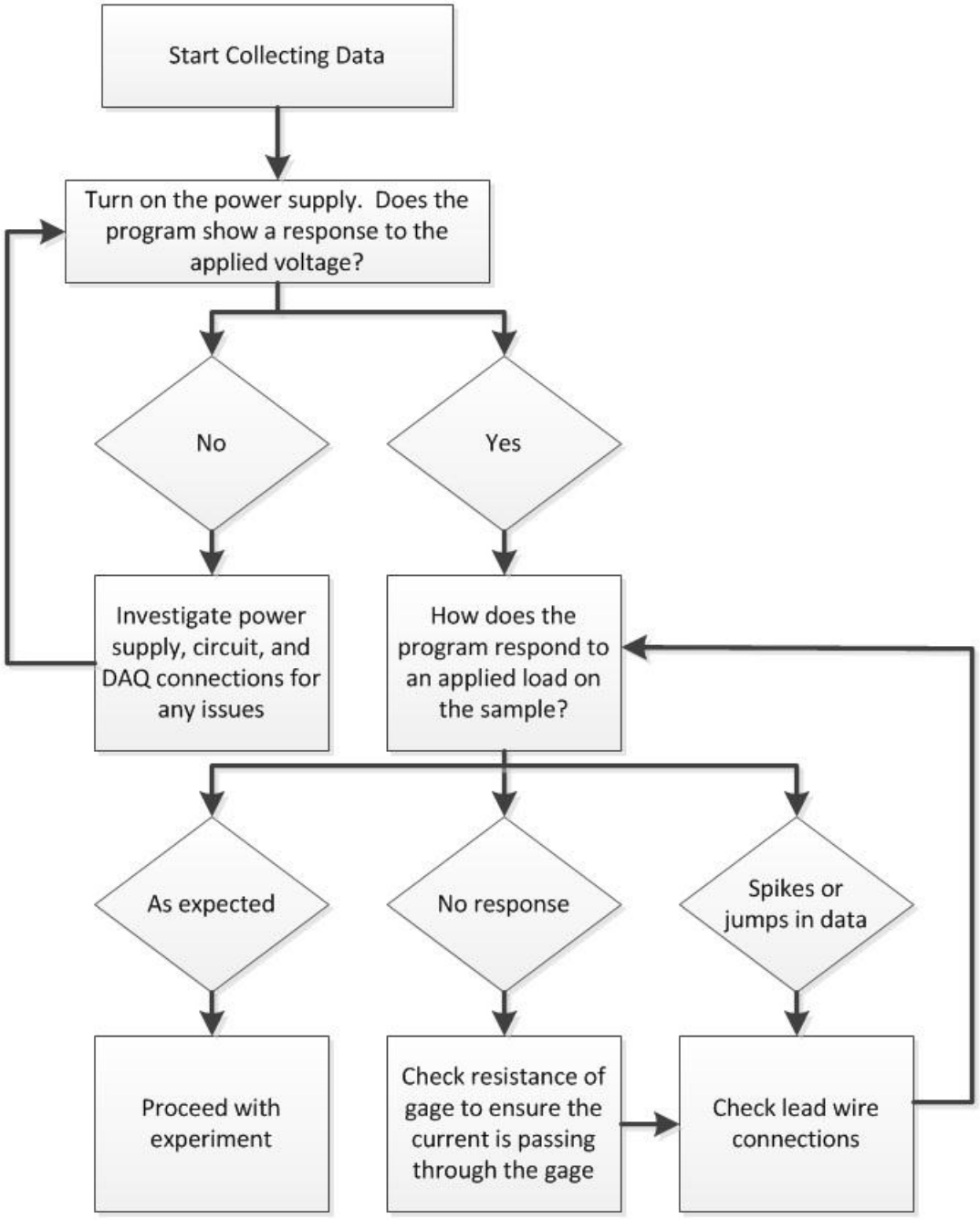

Figure 15. Troubleshooting logic table

SENSORS AND SIGNAL PROCESSING

The impetus of the project was to be able to utilize several off-the-shelf sensors in the blade design. A custom designed sensor would be ideal, however as was previously mentioned, cost is of utmost importance in the design and construction of the blades, and a series of custom built sensors would likely become prohibitively expensive. The sensors investigated were those that had been used during the previous set of experiments to test various mechanical effects of the material and an optimum way to treat the sensors before embedment. The actual sensors that were used are shown in Table 4. However, several other sensors were studied, to determine their practicality for future research.

Table 4: Sensors used for testing and embedment in composite samples

Type of Sensor	Type	Description
Metal Foil Strain Gage (MFSG)	KFG-5-120-C1-11L1M2R	5 mm grid, 120 ohms, 2 leads
	KFG-5-120-C1-11L3M3R	5 mm grid, 120 ohms, 3 leads
Polyvinylidene Fluoride (PVDF) Film	Measurement Specialties (LDT0-028K/L w/crimps)	25 mm long gage
	Measurement Specialties (LDT4-028K/L w/crimps)	170 mm long gage
Thermocouple	Type J	Iron – Constantan junction

Metal Foil Strain Gages (MFSGs)

One of the most common and practical strain sensors is the metal foil strain gage (MFSG) as seen in Figure 16. These sensors are relatively inexpensive and robust. The gages are simply a wire that is placed on a polymeric substrate, with several turns to

maximize the length of the wire in the longitudinal direction, since it is undesirable to have a transverse strain effect the response of the gage.

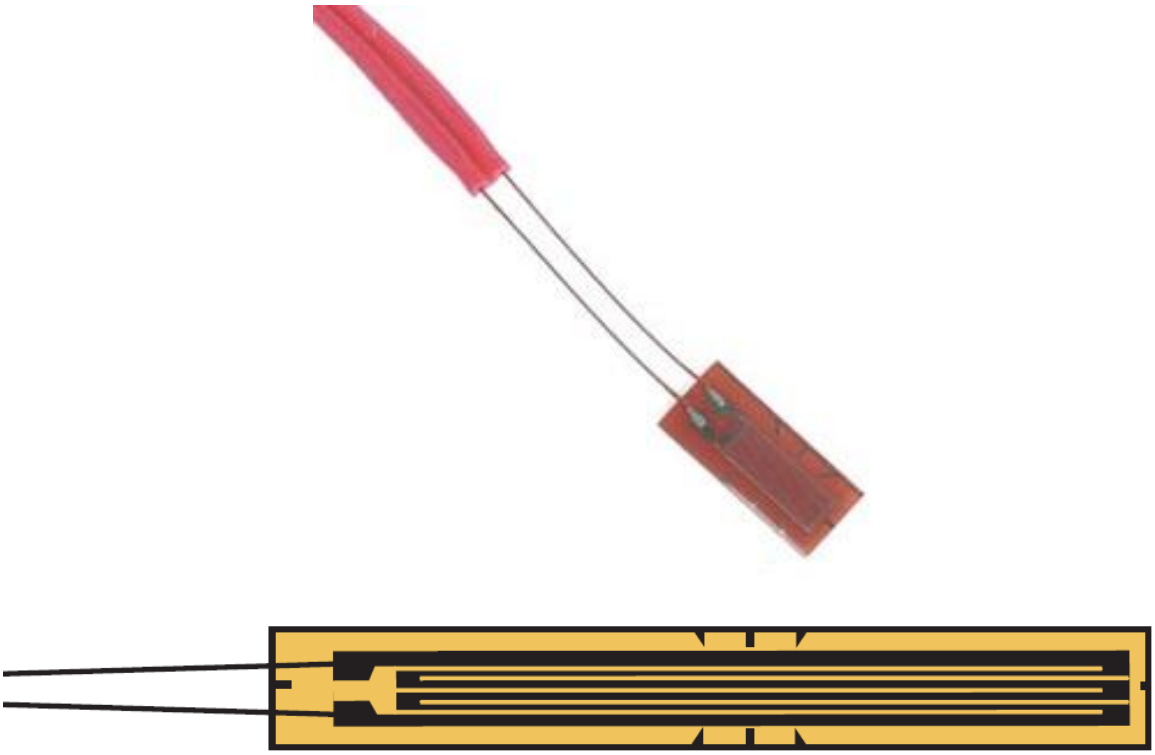

Figure 16. Metal Foil Strain Gage [16]

These gages work on the premise of a change in resistance of the wire, due to the change in length, cross-sectional area, and resistivity of the wire as shown in Equation 3 [17].

$$\frac{dR}{R} = \frac{d\rho}{\rho} + \frac{dL}{L} - \frac{dA}{A} \qquad \text{Equation 3}$$

Where

$R = resistance$
$\rho = resistivity$
$L = length\ of\ wire$
$A = cross\ sectional\ area\ of\ wire$

MFSGs come in many different shapes and sizes depending on the application, and the properties of the gages used are shown in Table 5.

Table 5. Strain Gage Properties

Type	KFG-5-120-C1-11L1M2R
Gage Factor	2.09 ± 1.0%
Gage Length	5 mm
Gage Resistance	120.4 ± 0.4 Ω

The Wheatstone Bridge

The change in resistance of a MFSG is typically very small and difficult to measure directly. Therefore, a Wheatstone bridge circuit, as shown in Figure 17 was used to amplify the response, and make it possible to measure the change. Since measuring a resistance is not very common in typical engineering practices, the Wheatstone bridge circuit is used to output a voltage that is proportional to the change in resistance of the strain gage. The Wheatstone bridge contains a resistor in each of the legs of the bridge with a resistance similar to the MFSG being used. The quarter bridge, where only one of the resistances is a MFSG is illustrated in Figure 17.

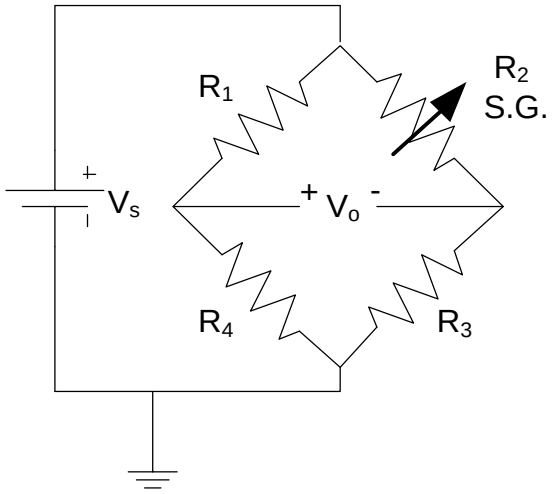

Figure 17. The Wheatstone bridge circuit used to amplify the MFSG signal.

From Equation 3 it is clear that the resistivity is also a factor in the overall resistance, but it does not change much under load. It is, however, affected by the temperature, which can cause erroneous readings which is the primary downfall of the quarter bridge. Therefore, a change in temperature will cause a change in the output voltage, and this can be misinterpreted as strain. One way to alleviate this issue is by using the half bridge [18]. The half bridge uses two strain gages as resistances in the bridge. As shown in Equation 4, it is possible to orient the two gages so that their changes in resistance subtract from one another (i.e. resistances 2 and 3). Therefore, a change in temperature that would create the same change in resistance would be canceled out.

$$V_o = \frac{V_s R_2 R_3}{(R_2 + R_3)^2}\left(\frac{\Delta R_3}{R_3} + \frac{\Delta R_1}{R_1} - \frac{\Delta R_2}{R_2} - \frac{\Delta R_4}{R_4}\right) \qquad \text{Equation 4}$$

Where

$V_o = output\ voltage$
$V_s = supply\ voltage$
$R_i = i^{th}\ resistance$

This can be problematic if the gages are placed so as to experience the same mechanical strain, as these readings would cancel each other out as well. Therefore, for a tensile test, one of the gages needs to be placed in a location of zero strain. This gage is than considered a dummy gage, since its only purpose is to compensate for temperature. Both gages can be active if the sample is undergoing bending, and the gages are located on opposite sides of the sample so as to be subjected to the same magnitude of strain, but opposite direction (tension/compression).

This leads to one of the primary objectives of this project, the separation of mechanical and thermal strain, so as to measure the temperature and mechanical strain using only one type of sensor. It has been proposed that by using one quarter bridge, both the apparent thermal and mechanical strains will be measured. The half bridge with a dummy gage will only measure the mechanical strain. By looking at the difference between these two measurements, only the thermal strain will be left. Ideally, this thermal strain will be proportional to the temperature of the sample being tested. The wiring diagram of the two different bridges is shown in Figure 18.

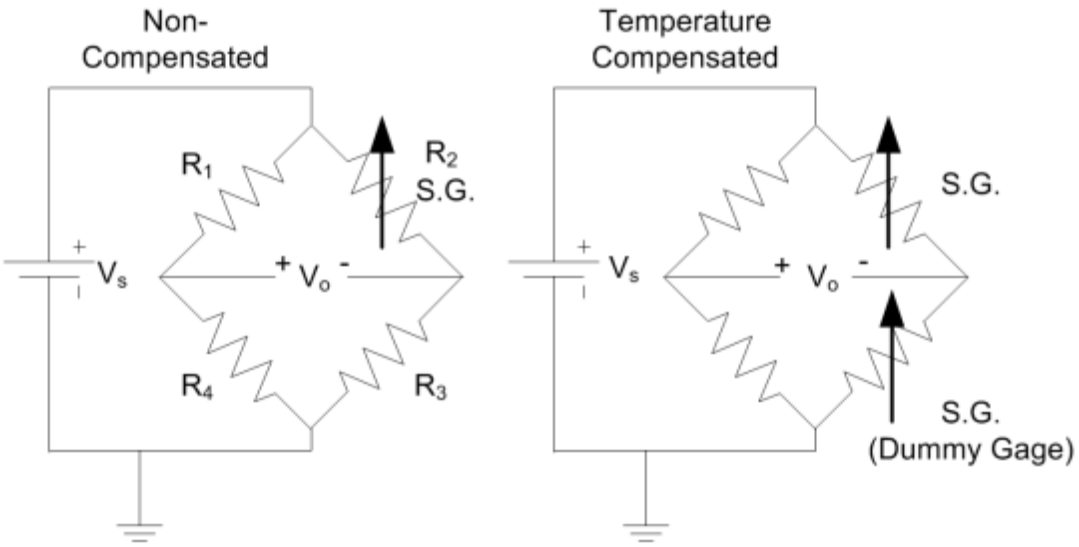

Figure 18. The quarter bridge and half bridge used to separate the mechanical and thermal strains

It is simple enough to compensate for the change in temperature of the gage itself; however, issues also arise from the heating of the lead wires attaching the gage to the circuit. Just as with the wire on the gage itself, the lead wires adhere to Equation 3, and the resistivity changes with temperature. This is typically only an issue with long lead wires, however, it was noticed that even a short section of wire heated quickly greatly affected the results. Therefore, a 3-wire type strain gage was implemented to negate the lead wire resistance issue. This 3-wire type gage was only needed for the quarter bridges, as the half bridges already compensated for this error.

The 3-wire connection works because R_{L1} and R_{L3}, as shown in Figure 19, are in adjacent legs of the bridge. So by using Equation 4, the temperature affects in each of these lead wires cancel each other out. Since R_{L2} is attached to the DAQ, very little current is drawn, so any change in resistance is negligible,

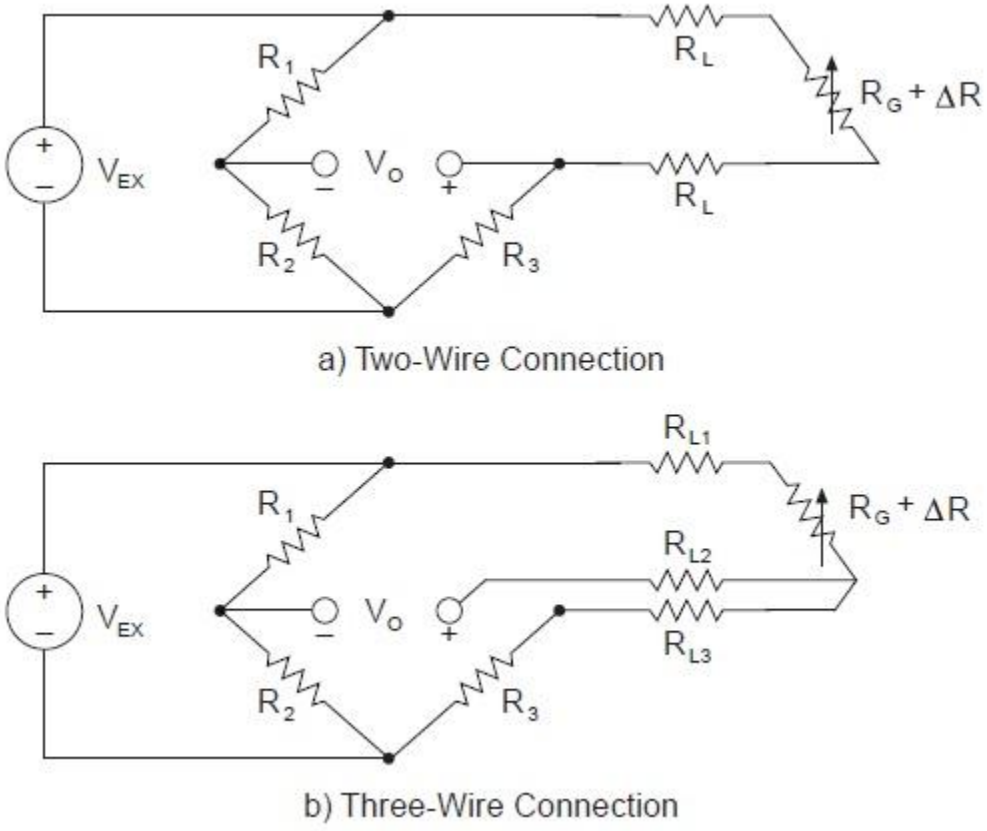

Figure 19. Two-wire vs. three-wire strain gage in Wheatstone bridge [19]

Relating the strain to the output voltage is obtained by performing a circuit analysis on the Wheatstone bridge as shown in any instrumentation book. The transformation for a quarter bridge is described in Equation 5, but as the half bridges used contained a dummy gage under no strain, the same equation applies to these bridges.

$$\varepsilon = \frac{-4V_r}{GF(1+2V_r)} \qquad \text{Equation 5}$$

Where

$$V_r = \frac{V_{o(strained)} - V_{o(unstrained)}}{V_s}$$

$$GF = gage\ factor$$

Strain Gages on Composites

One important attribute of using strain gages on composite materials that needs to be addressed is the orthotropic nature of the material. Strain gages were designed to be used with isotropic materials, as very few engineering materials were orthotropic when the gages were being developed. This causes complications because of the difference in thermal expansion, and modulus of elasticity from the longitudinal to the transverse direction [20].

The alignment of the gage also plays a large role in accurately measuring strain. As all of the specimens used in testing were unidirectional glass fiber composites, the error was similar to that produced by an isotropic material as shown in Equation 6

$$\frac{(\varepsilon_x' - \varepsilon_x)}{\varepsilon_x} = -(1 + \nu_{12})sin^2\beta \qquad \text{Equation 6}$$

Where

$\varepsilon_x = strain\ along\ x\ direction$
$\nu_{12} = Poisson's\ ratio$
$\beta = fiber\ misalignment\ angle$

When utilizing strain gages with metallic material, a single gage can be selected that is already temperature compensated to the material being used. The strain gages that were used for the experimentation were tailored for use on steel structures. But it is the orthotropic nature of the composites that again prevent an easy solution to temperature compensation. A gage could be designed to work on composites, but it would only work for a specific fiber/matrix combination, and only for a specific gage alignment [21].

Many of these issues were not as critical as they could become due to the use of uni-directional composites. This made it much easier to line up the strain gages, and use a calculated value for Poisson's ratio.

Polyvinylidene Fluoride (PVDF) Film

Another sensor that has become important in the field of sensing pressure and strain is the piezoelectric film. A piezoelectric material is one that generates an electrical charge when deformed. Some of the most common types of piezoelectric materials are quartz, Rochelle salt, and barium titanate, which was the first piezoelectric ceramic discovered. These materials are all crystalline, which is the source of their piezoelectric properties. PVDF is unlike these materials in that it is a polarized polymer rather than a ceramic material. The cross section of the PVDF film, in which the silver ink acts as electrodes to hold the charge developed by the PVDF is illustrated in Figure 20. The Mylar provides a layer of protection for the electrodes against the environment.

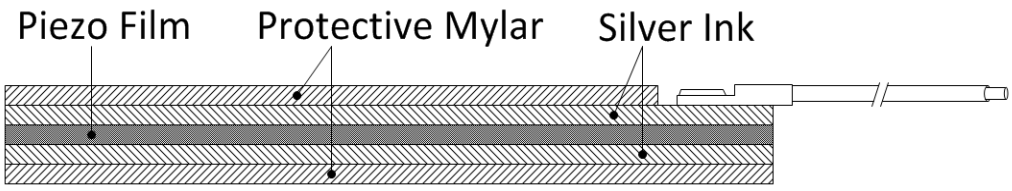

Figure 20. The cross-sectional view of the PVDF film

Piezoelectricity

As mentioned earlier, the crystalline structure is part of what gives ceramic piezoelectric materials their piezoelectricity. PVDF is a semi-crystalline polymer, which

means its structure is much more random, but it still uses similar mechanisms to generate its charge.

Pyroelectricity

One of the properties of PVDF films that make them difficult to use in constantly changing environments is the pyroelectric nature of the polymer. Pyroelectricity, much like piezoelectricity, is the ability of a material to develop a charge due to a change in temperature. The heating causes the dipoles to have a random motion that reduces the polarization of the film [22]. This feature has allowed them to be used in motion sensing devices. Several of the properties mentioned previously are shown in Table 6.

Table 6. PVDF film properties

Property	Symbol	Value	Units
Piezo Strain Constant	d_{31}	23	10^{-12} $(C/m^2)/(N/m^2)$
	d_{33}	-33	
Pyroelectric Coefficient	P	30	10^{-6} $C/m^2*°K$
Temperature Range		-40 to 80	°C
Capacitance	C	380	pF/cm^2

Charge Amplifier Circuit

The PVDF film sensors are very sensitive to small changes in strain, but since they develop a charge, and not a voltage due to some external event, they are not optimum for steady state or static measurements. Rather, they are very useful for dynamic events, such as impact or vibration measurements. They can also be used for acoustical emission testing, which is very important in composite health monitoring [23].

The charge that the PVDF film generates is much like the resistance of the MFSG, in that it is not a simple quantity to measure. This leads to the need of a circuit that can convert the charge into some type of easily measured value. The circuit that is most frequently used in sensing the response from a PVDF is the charge amplifier circuit as shown in Figure 21.

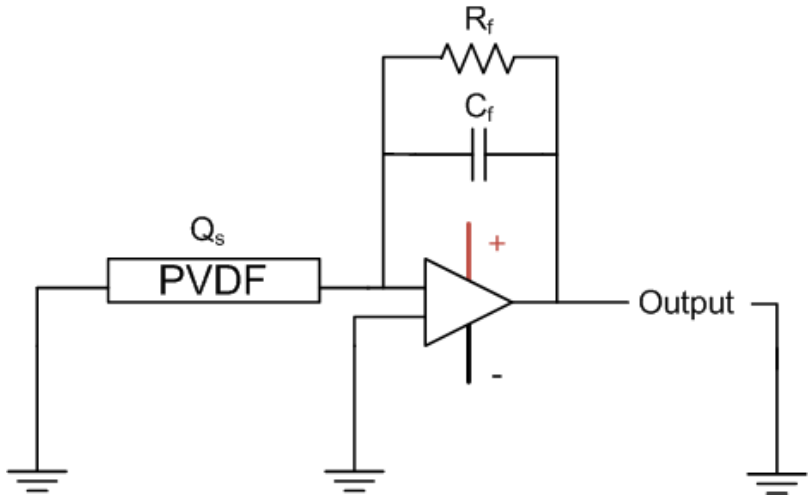

Figure 21. Charge Amplifier Circuit

Some of the important quantities from this circuit are the time constant and output voltage as described in Equation 7 and 8.

$$\tau = C_f * R_f \qquad \text{Equation 7}$$

$$V_{out} = -\frac{Q_s}{C_f} \qquad \text{Equation 8}$$

Where

$\tau = time\ constant$
$R_f = feedback\ resistance$
$C_f = feedback\ capacitance$
$Q_s = charge\ developed\ on\ PVDF$

To eliminate the thermal effects on the gage, a dual gage configuration was used to cancel out the charges developed on the PVDF film. Since the PVDF film gages have a positive and negative electrode, the signals can be added or subtracted from one another by placing them in front of the charge amplifier circuit. The method in which the dual configuration is wired with respect to the charge amplifier circuit is shown in Figure 22.

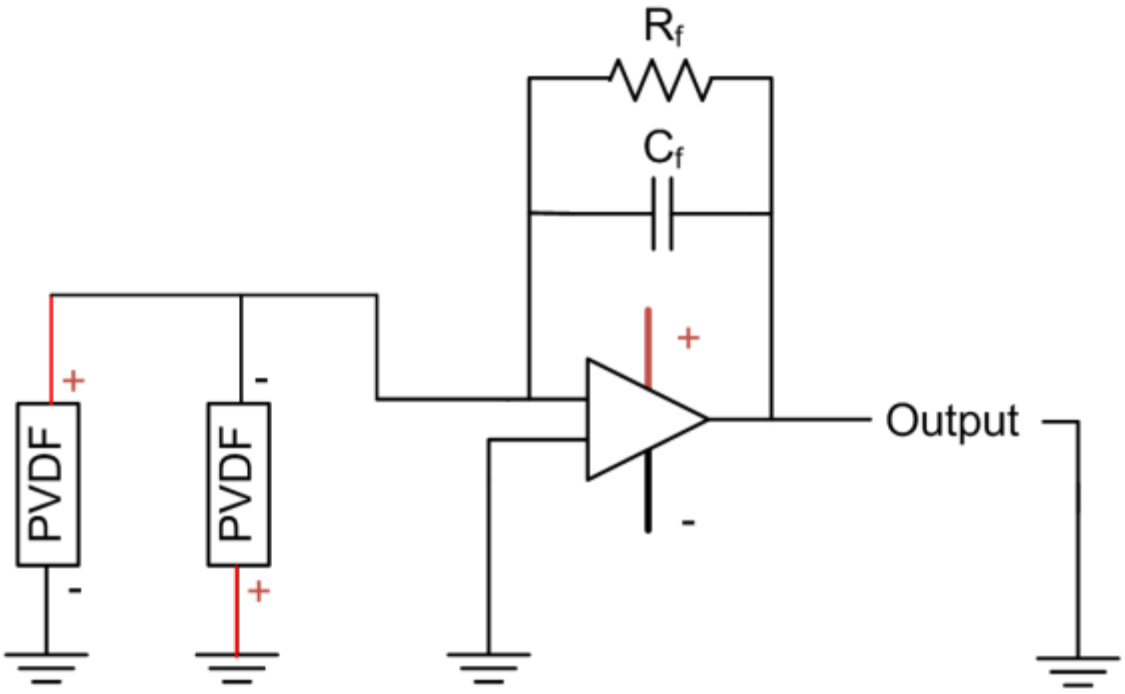

Figure 22. Dual gage configuration used to remove the thermal response of the sensors

Comparable to the half bridge circuit used to cancel out the thermal effects of the MFSGs, this circuit will also cancel out mechanical effects if both of the PVDF films undergo the same mechanical loading. Therefore, one of the gages needs to be setup as a dummy gage so as to be subjected to the same thermal environment but not exposed to any of the mechanical loading.

Thermocouples

Thermocouples are another very simple sensor that provides accurate results with minimal signal processing. They consist of two dissimilar metals bonded with a wire bead. According to the Seebeck effect, an electromotive force is created due to a temperature difference at the manufactured junctions [24]. As shown in Figure 23, this relationship is typically linear, especially for low temperature applications.

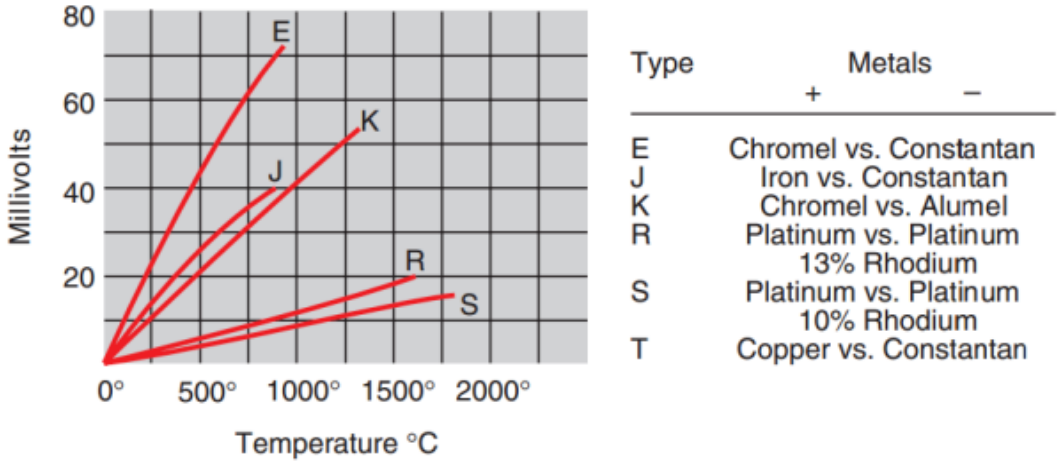

Figure 23. Thermocouple temperature vs. voltage generated [25]

The thermocouples used for all of the experiments were type J. These thermocouples have a range from -40 to 750 °C, which is quite a bit less than most of the other thermocouples. However, since the composites should not be exposed to temperatures above their oven cure temperature (typically around 80 °C); there is not much of a problem with this limitation.

The typical method for manufacturing these sensors, assuming the wire is already pre-manufactured, is to create a single bead at the tip of the two wires, and leave the junction exposed. This solution is fine for measuring gaseous environments, but once

embedded; the thermocouples with exposed beads were registering a value several degrees higher than what was known (room temperature). A new method was implemented in which the two wires were first soldered together, rather than just a single bead, to create a more robust connection. This junction was then covered over with heat shrink tubing and a dab of silicone sealant to protect the junction from the resin.

Fiber Optics

Fiber optics have recently become more desirable for use in measurement systems. This interest has stemmed from a reduction in cost of these systems. In the past, these have been too expensive to use for commercial purposes. Advancements in telecommunication have lowered the cost of most of the components required in utilizing fiber optics. Therefore, the feasibility of using fiber optics as sensors has become a reality. Previous work at MSU has dealt with embedding fiber optic sensors in composite materials. However, these sensors were not utilized during the sensor work presented in this thesis. The following information is provided as a qualitative assessment of these gages to complement the previous work performed, and the possibility of using these sensors for future work on this topic.

Advantages of Fiber Optics

Unlike the MFSGs and PVDF films, fiber optics have been proven to accurately measure temperature, and not just by utilizing the error component of thermal effects on the gage. Due to the different types of fiber optics, there are many different parameters that fiber optics can measure. The size of the fiber is also desirable when compared to

the other sensors investigated since a typical fiber is several hundred microns in diameter and would therefore not be as intrusive in the material. These features make them very attractive as an embedded sensor.

Multiplexing is another feature that is appealing in fiber optic systems. Multiplexing allows multiple signals to be combined into a single analog signal, and then reversing the process to see each individual signal at the processing unit. This allows multiple measurement locations along a single fiber, where individual strain gages (along with their Wheatstone bridge circuit) would be needed for each location to achieve similar results. Some companies have claimed up to 1 cm spatial resolution up to 70 meters along a single fiber. This kind of spatial resolution with accuracy of ±1 μstrain and ± 0.1 °C is very desirable for structural monitoring [26]. There are multiple types of multiplexing such as frequency division multiplexing and wavelength-division multiplexing as illustrated in Figure 24. As illustrated in the figures, the different wavelengths or signals are initially split at the multiplexer, travel through the fiber, and are then combined again once they have passed through.

Advanced Types of Fiber Optic Sensors

Fiber optic cables allow light to pass through the cable based on the internal refractive index of the fiber. If the light comes in at an angle to steep, it will not be reflected, and can no longer continue through the material.

The basic fiber optic cable is the most simple of the fiber optic sensors and is affected by micro bending. This micro bending causes a change in the refractive index of

the fiber. Therefore, this method can measure strains caused by bending or localized loading conditions as shown in Figure 25, not axial strains.

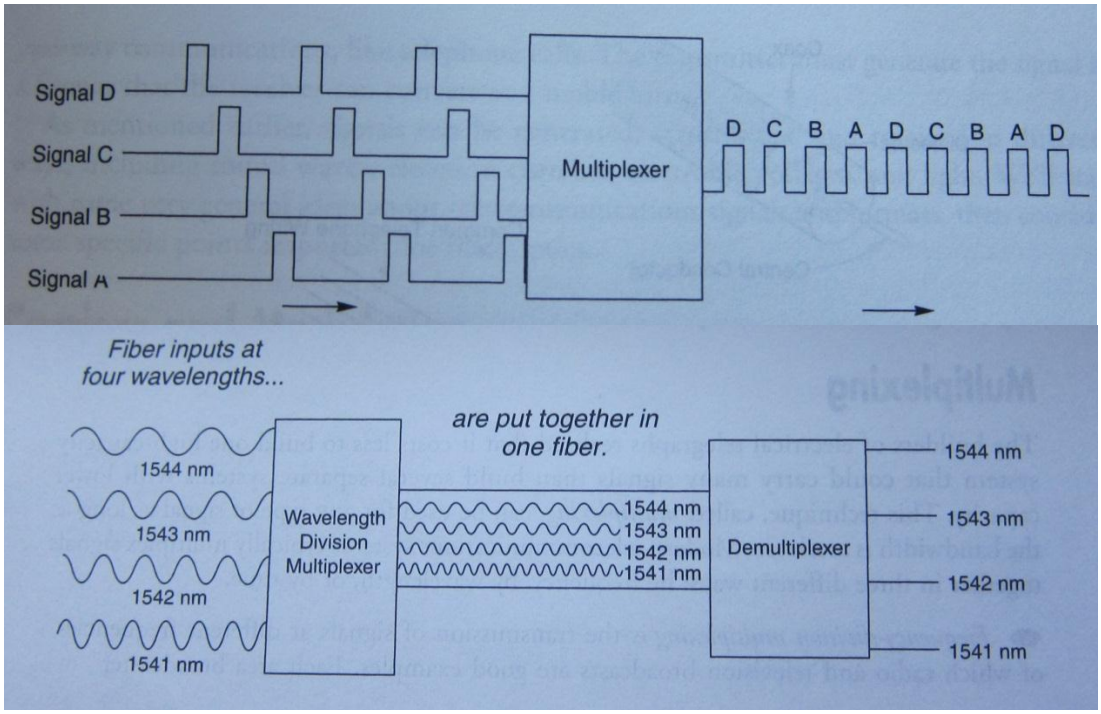

Figure 24. Wavelength-division (top) and Time-division (bottom) multiplexing

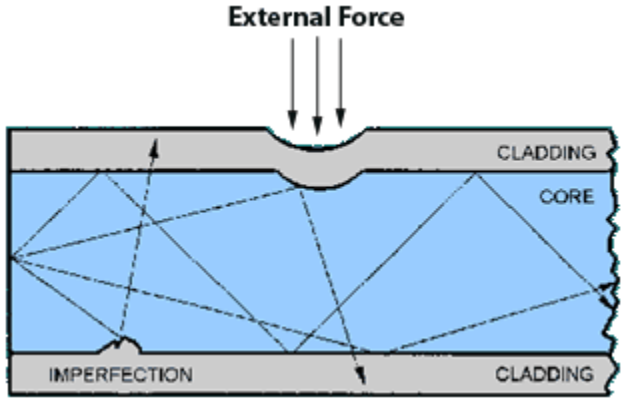

Figure 25. Basic fiber optic cable [27]

Fiber Bragg Grating: The primary type of fiber optic sensor that has been implemented in composite materials is the Fiber Bragg Grating (FBG) sensor as seen in

Figure 26. This type of fiber has intra-core grating which causes the scattered light to constructively add together with a central wavelength known as the Bragg wavelength. Since the Bragg wavelength is dependent on the spacing of the grating; it is a function of the strain, and is affected by both axial loads, as well as bending loads.

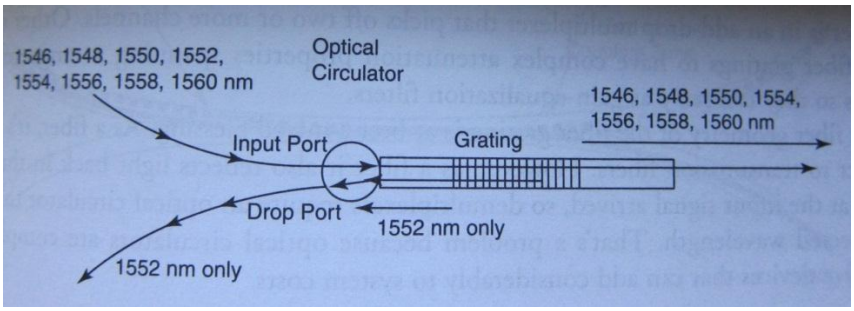

Figure 26. Example of Fiber Bragg Grating

Extrinsic Fabry-Perot Interferometer (EFPI): The EFPI is fiber optic sensor that uses two optical fibers contained in a capillary tube with a small gap of roughly 50 µm between the two fibers [28] as illustrated in Figure 27. As the light reaches the end of the primary fiber, a portion of the light is reflected, while the majority passes through the gap. Both of these signals return to the receiver, but with a phase difference due to the gap. Any strain experienced by the capillary tube will alter the gap length, and in turn the phase angle will change.

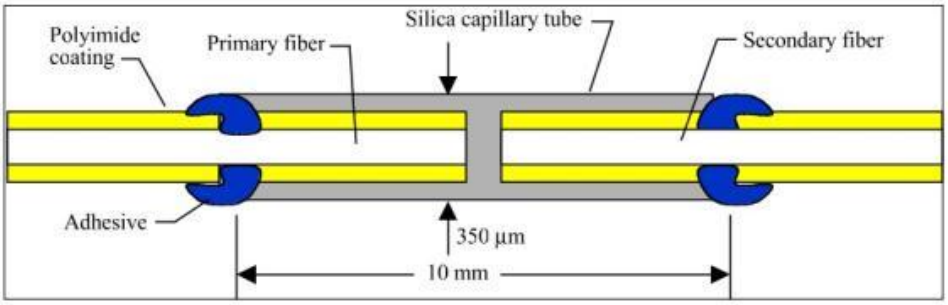

Figure 27. EFPI Sensor [28]

Several groups [28, 29] have designed experiments to simultaneously measure strain and temperature, which is the goal of MSU's embedded sensor research. They utilize a coefficient matrix style solution to measure the change in the Bragg wavelength, and reflected spectrum similar to Equation 9.

Another method that has been developed to simultaneously measure both strain and temperature is to use a combination of the EFPI and FBG concepts. Multiple papers have been published on the ability of these hybrid sensors to accurately measure both quantities [30, 31]. A version of the hybrid sensor used in these tests is illustrated in Figure 28. The capillary tube that surrounds the optical fiber isolates the sensor from external strains. Therefore, it is only affected by changes in temperature. The EFPI portion of the sensor is subjected to both the temperature and mechanical strain of the material. The relationship derived between the measurable values is described in Equation 9. The P coefficients can all be analytically derived.

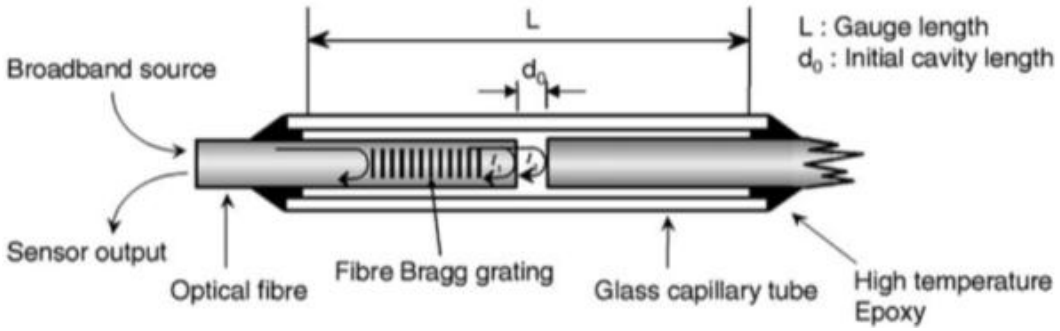

Figure 28. FBG/EFPI hybrid sensor [32]

$$\begin{Bmatrix} \varepsilon \\ \Delta T \end{Bmatrix} = \begin{bmatrix} P_{1\varepsilon} & P_{2\varepsilon} \\ P_{1T} & P_{2T} \end{bmatrix} \begin{Bmatrix} \Delta d \\ \Delta \lambda_B \end{Bmatrix} \quad \text{Equation 9}$$

Where

$P_{i\varepsilon} = strain\ related\ coefficients$
$P_{iT} = temperature\ related\ coefficients$
$d = EFPI\ gap\ length$
$\lambda_B = Bragg\ wavelength$

Luna technologies, who have contacted MSU about possible future collaborations, have developed many systems for monitoring stain and temperature. Their primary method is through the use of Rayleigh scatter-based measurement. One of the more interesting approaches that they have taken is by using a standard polarization maintaining fiber, which involves inducing residual stresses in the fiber, rather than the FBG or EFPI altered fibers. They use a similar methodology to the coefficient matrix solution, recognizing that the change in temperature or strain will shift the scatter pattern from the section of fiber. High-sensitivity Optical Frequency Domain Reflectometry is used to measure this scatter [33]. The backscatter is caused by the random surface fluctuations in the fiber that alter the index of refraction [34]. These systems have been shown to have resolution of 3.5 C and 35 μstrain. The achievable accuracy of this system is not as good as the FBG sensors, but the savings in cost makes them a very attractive option for structural health monitoring of blades.

Data Acquisition and Signal Processing

All data was acquired through an NI-DAQ USB 6229. The LabView program only recorded the raw data, so that if there were any discrepancies between the data and the expected results, it can be shown that it was not a problem from data processing in the

program. The program was designed so that any signal could easily be read by changing a few key aspects in the DAQ Assist menu. These features are shown in Table 7

Table 7. DAQ Assist settings

Signal	Min	Max	Other
Input Voltage	-10 V	10 V	Differential Measurement
MFSG	-50 mV	50 mV	Differential Measurement
PVDF	-10 V	-10 V	Differential Measurement
Thermocouple	0 C	100 C	25 CTC

The block diagram developed for capturing the raw data is shown in Figure 29 and Figure 30.

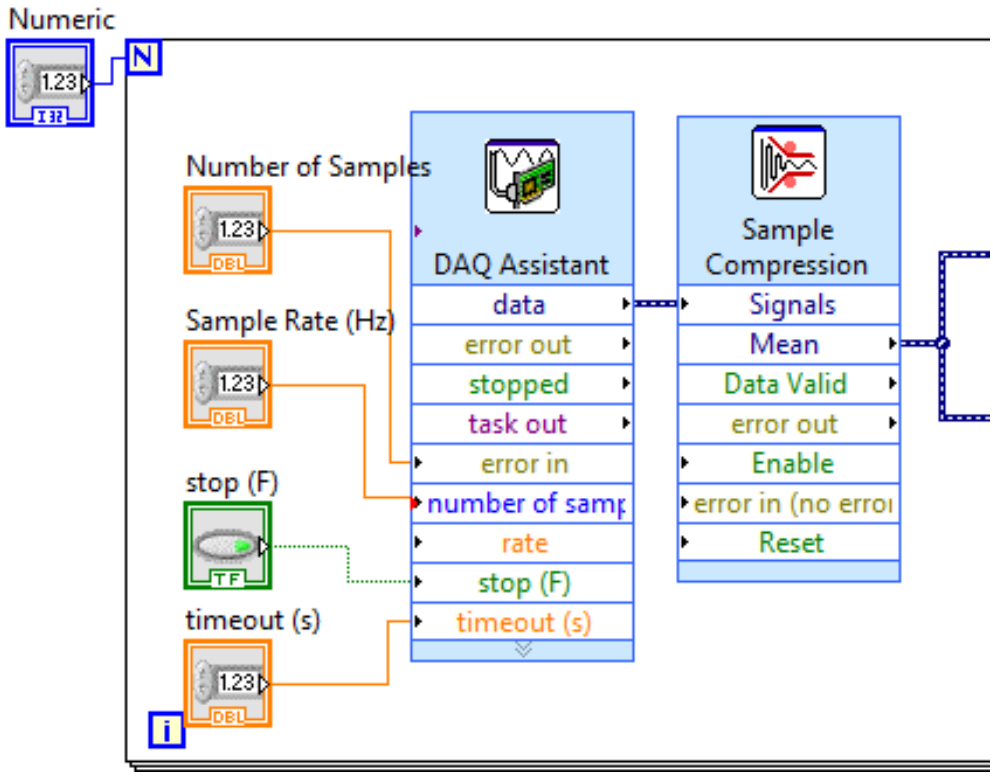

Figure 29. General collection of data program - LabView Screenshot (Part 1 of 2)

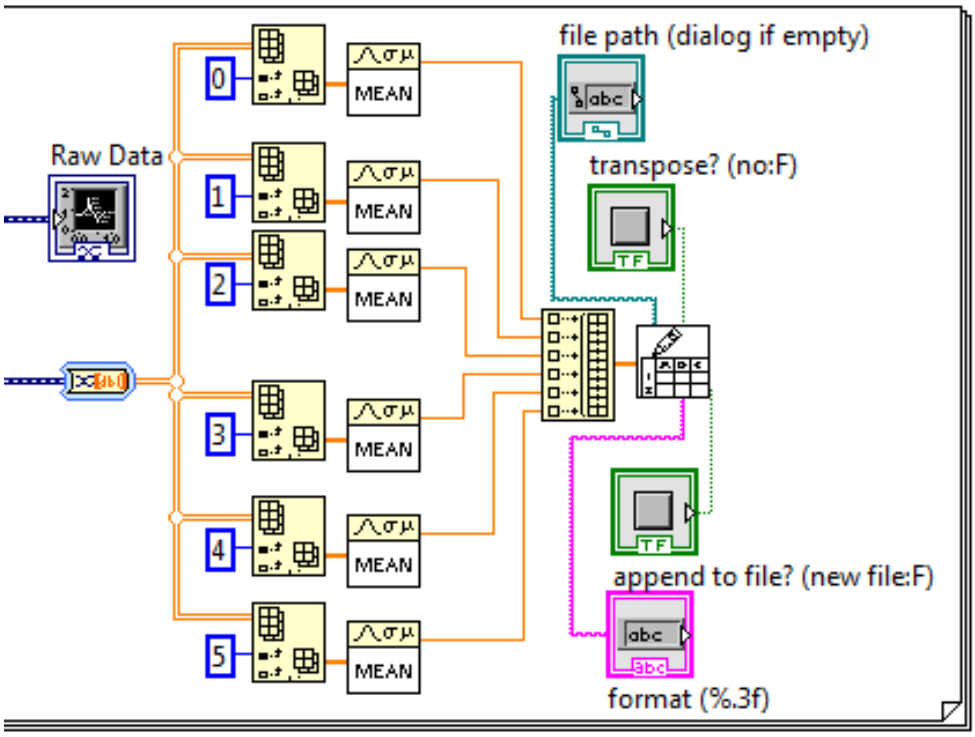

Figure 30. General collection of data program - LabView Screenshot (Part 2 of 2)

The post processing was handled in LabView as well. A program was created that would read a text file, and plot all of the raw data, so as to make sure there were no anomalies in the original file. Using the equations previously developed, the voltages were converted into their corresponding strains, and then re-plotted. An option was designed into the program to only save data when everything looked right, so as not to create several unnecessary files. The block diagram of the program is shown in Figure 31 -Figure 33.

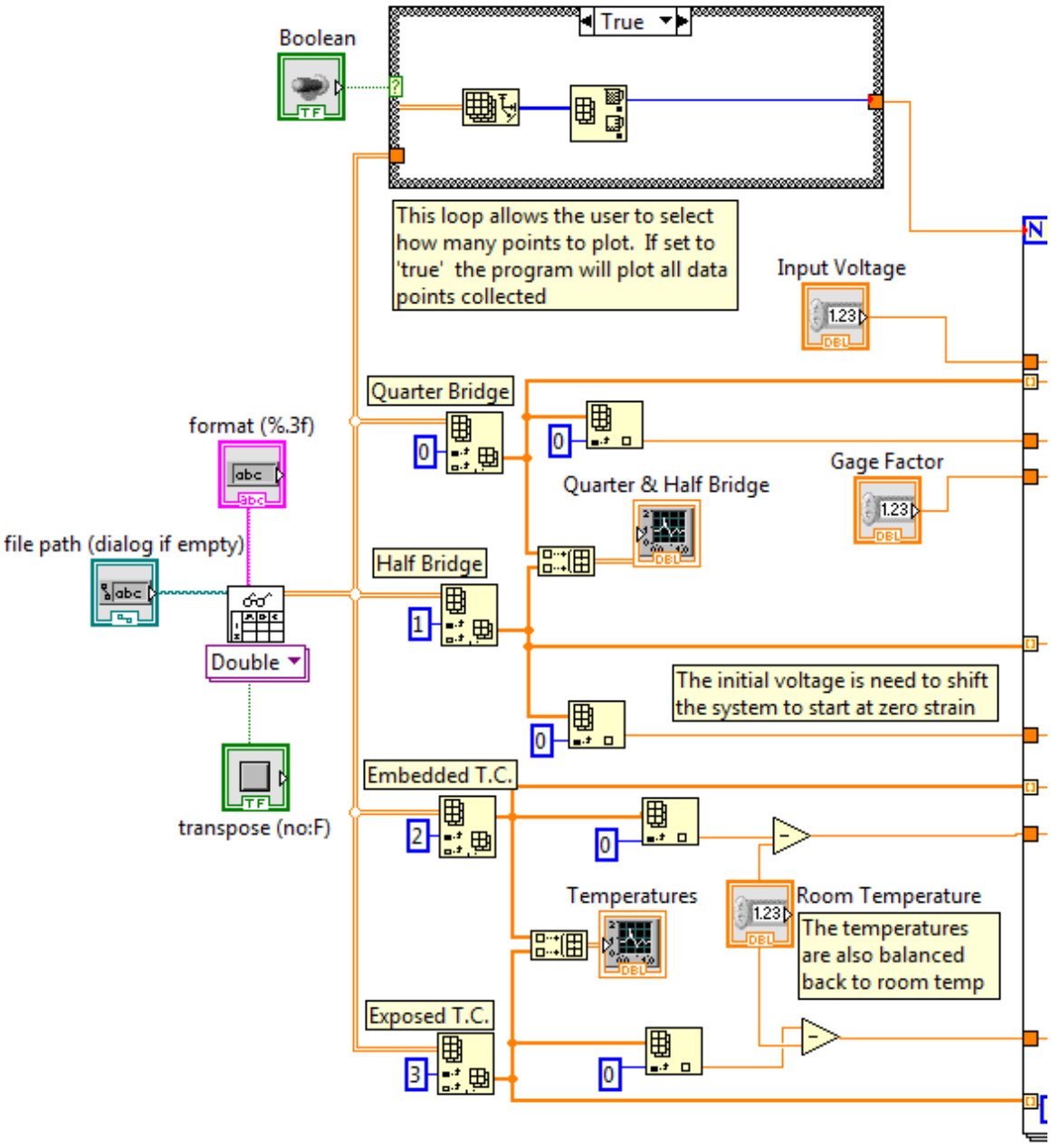

Figure 31. Post processing program - LabView Screenshot (Part 1 of 3)

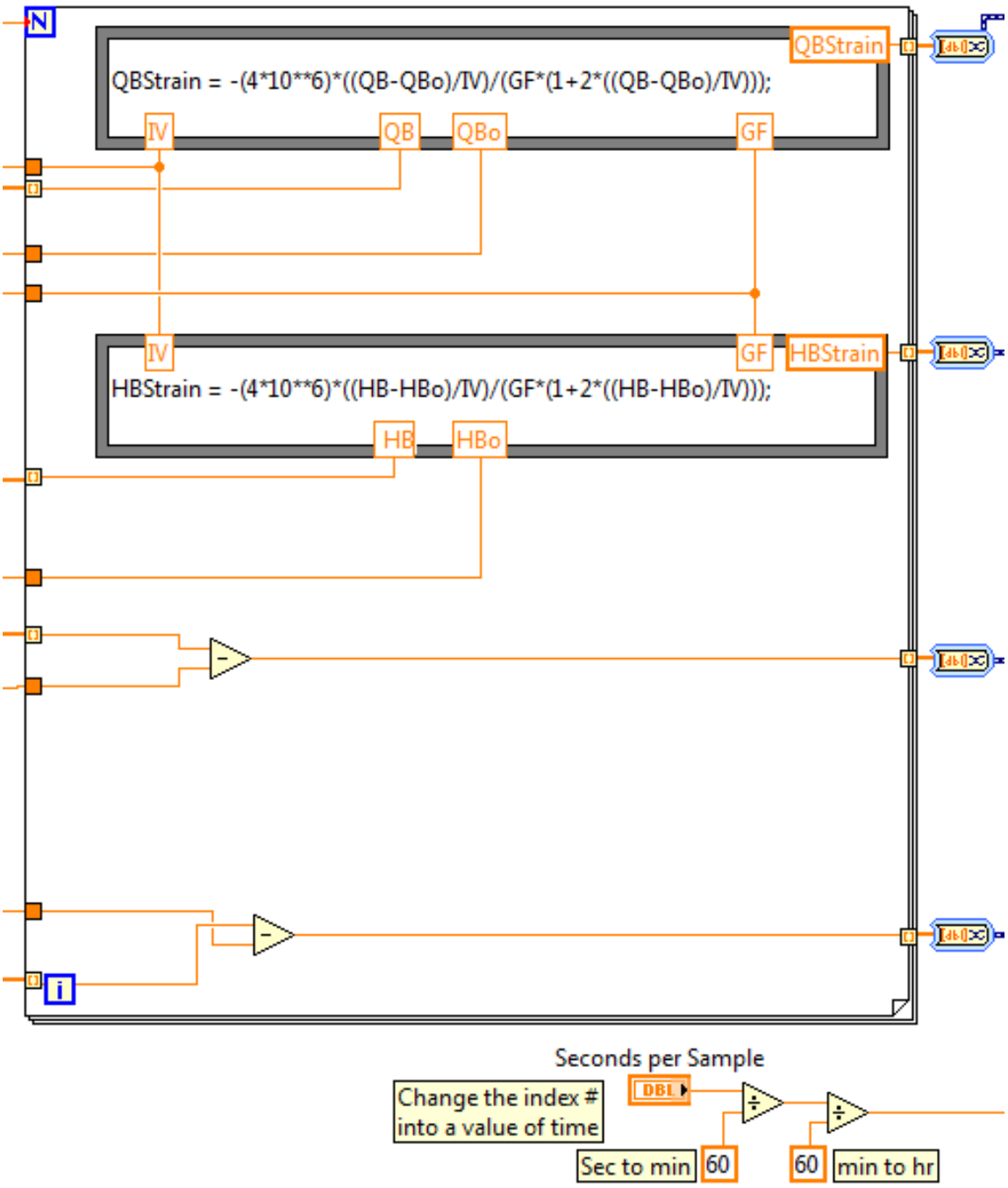

Figure 32. Post processing program - LabView Screenshot (Part 2 of 3)

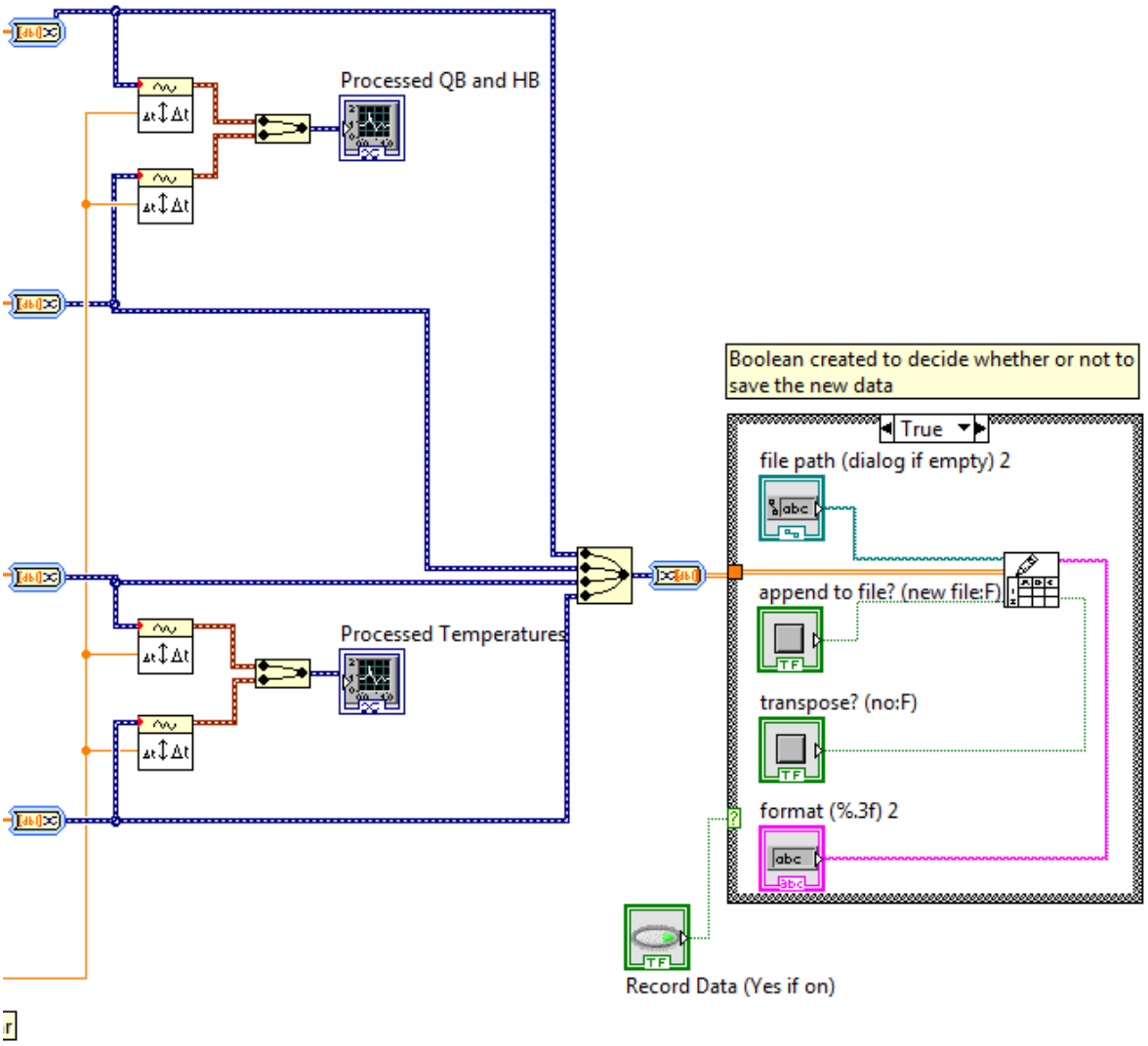

Figure 33. Post processing program - LabView Screenshot (Part 3 of 3)

MANUFACTURING COMPOSITES WITH EMBEDDED SENSORS

The VARTM Process

The process for building the Glass Fiber Reinforced Polymer (GFRP) is incredibly labor intensive. A process known as Vacuum Assisted Resin Transfer Molding (VARTM) was the method used for saturating the glass fibers with the epoxy. The specifications of the composite built are shown in Table 8.

Table 8. Components of glass fiber composite as built

	Manufacturer	Specification
Fiber	Saertex uni-directional	U14EU920-00940-T1300-100000
Matrix	Gurit	Prime 20LV Resin

Following the recommendations of the previous researcher, the sensors were treated by cleaning them with isopropyl alcohol, then submerging them in a 20% by weight nitric acid solution for 10 seconds, then rinsing with water. The sensor preparation station used to treat the gages is shown in Figure 34.

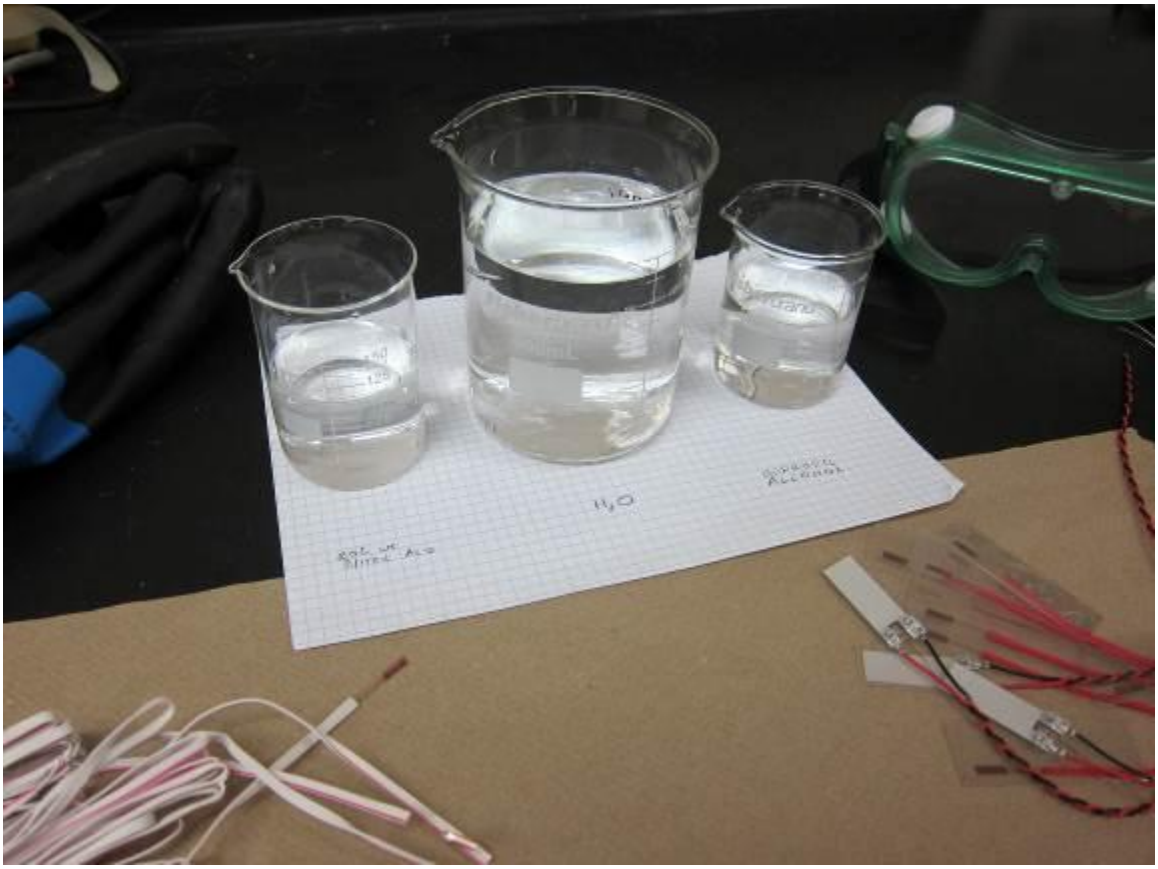

Figure 34. Sensor treatment setup containing isopropyl alcohol, water, and 20% by weight nitric acid

Before building up the composite, the aluminum plate that the composite was built on needed to be prepared. This included cleaning off all of the excess resin from the previous plate that was made, drilling out the inlet and outlet ports from the resin buildup, and adding all of the appropriate hoses for the vacuum and inlet of the resin/epoxy. A thin coat of mold release was also used to prevent the resin from adhering to the aluminum plate. After the plate was properly prepared, the composite could be built up.

The first layer that was applied was a sheet of peel ply. This material makes it much easier to remove the composite from the aluminum plate near the end of fabrication. The sheet of peel ply was taped down so as not to allow it to shift while the

following layers were added. Next, a border of "Tacky Tape" was lain down around the peel ply with a spacing of approximately 5 cm. This tape was the adhesive bond between the aluminum plate and the vacuum bag, but was also useful as a reference for the early stages of layup. The aluminum plate, after these layers had been applied, is shown in Figure 35.

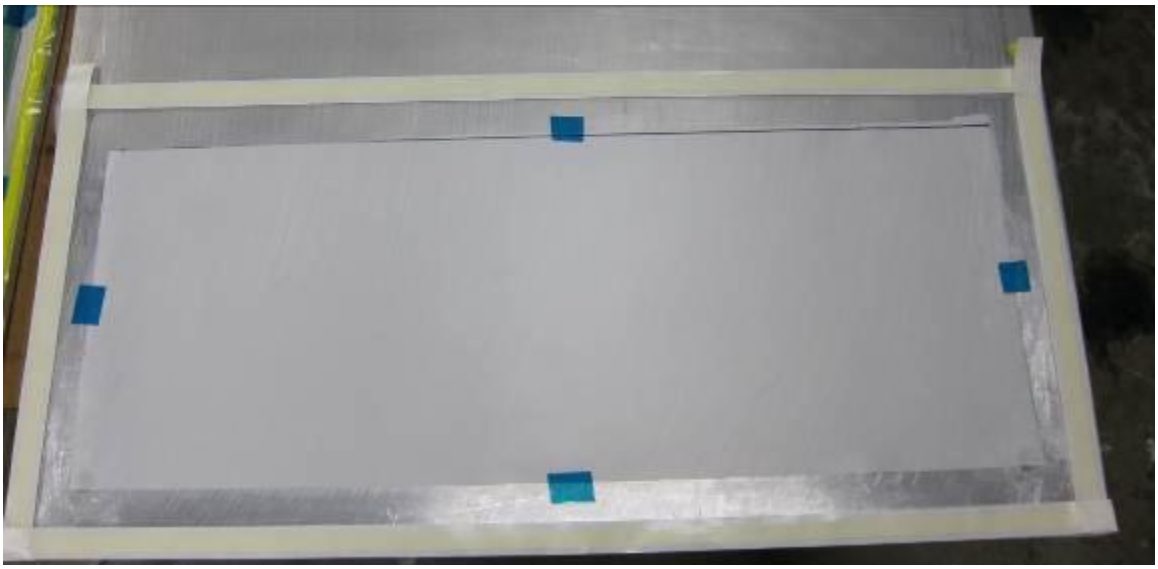

Figure 35. Aluminum mold with peel ply and tacky tape applied

On the layup table, a separate location for preparing and cutting material, the sheets of glass fiber were lain down, one at a time, ensuring that there were no obvious material defects with the sheet, such as in-plane waviness, and making sure it laid flat. The sheets that were to be below the gages were all stacked and the outline for where the sensors would be placed and the sample geometry were traced on the top sheet. Super 77, a 3M aerosol adhesive was used to attach the sensors to the fiber glass at the prescribed positions. The gages, as adhered to the glass fibers, are illustrated in Figure 36.

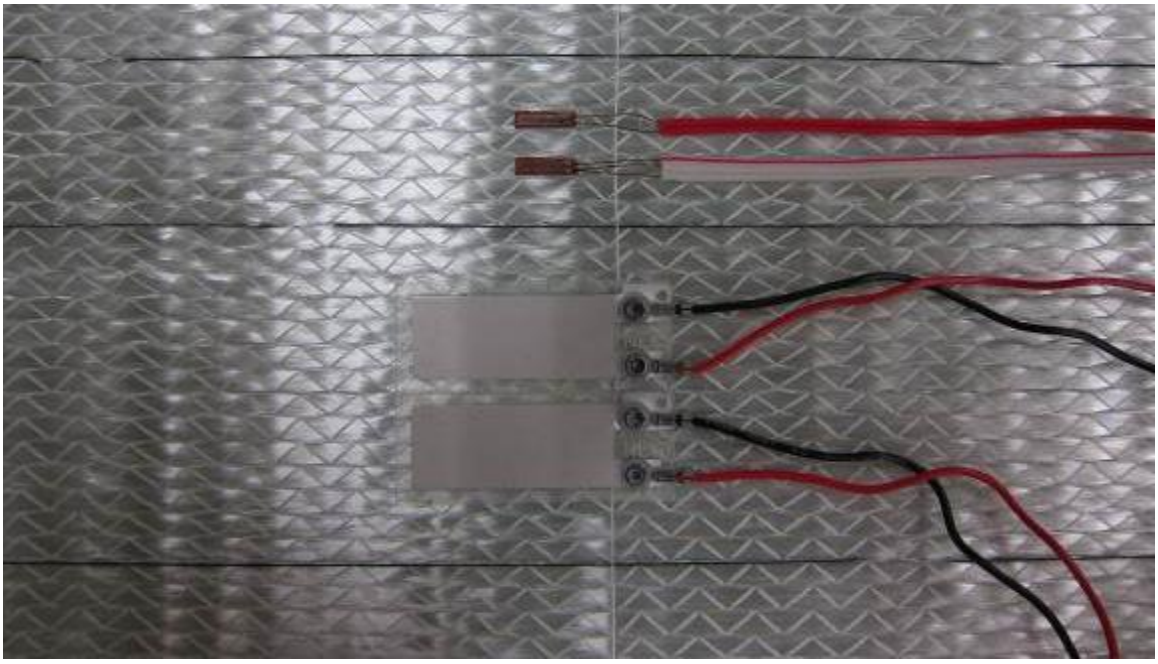

Figure 36. Two of the PVDF films and two of the MFSGs as adhered to the glass substrate

Once all of the sensors had been placed, the 4 layers of glass fibers along with the sensors were moved to the aluminum mold plate and taped down. All of the lead wires were placed away from the centerline to make the process of extracting the wires from the fibers more simple. Once the sensors were glued down, the sheets were left overnight to allow the adhesive to dry completely.

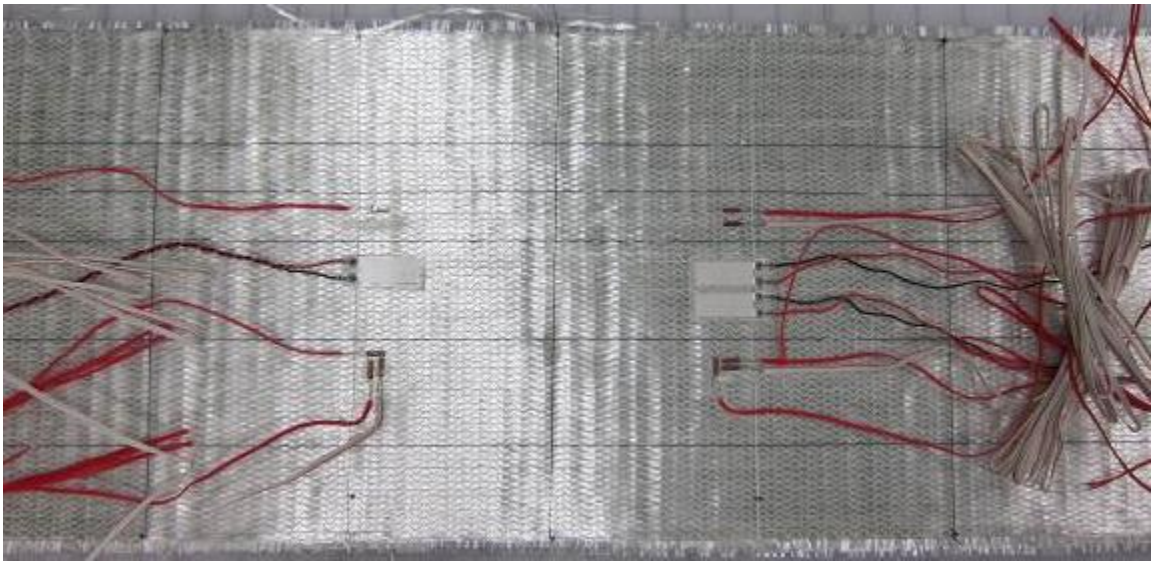

Figure 37. The top view of the sensors as adhered to the glass fibers

To get the wires to the surface of the composite, the lead wires needed to be threaded through the individual tows of the next layer as shown in Figure 38. This is a very tedious and time consuming process, but in a full scale blade, it is expected that the lead wires would run through the length of the blade while still embedded in the composite, rather than coming to the surface.

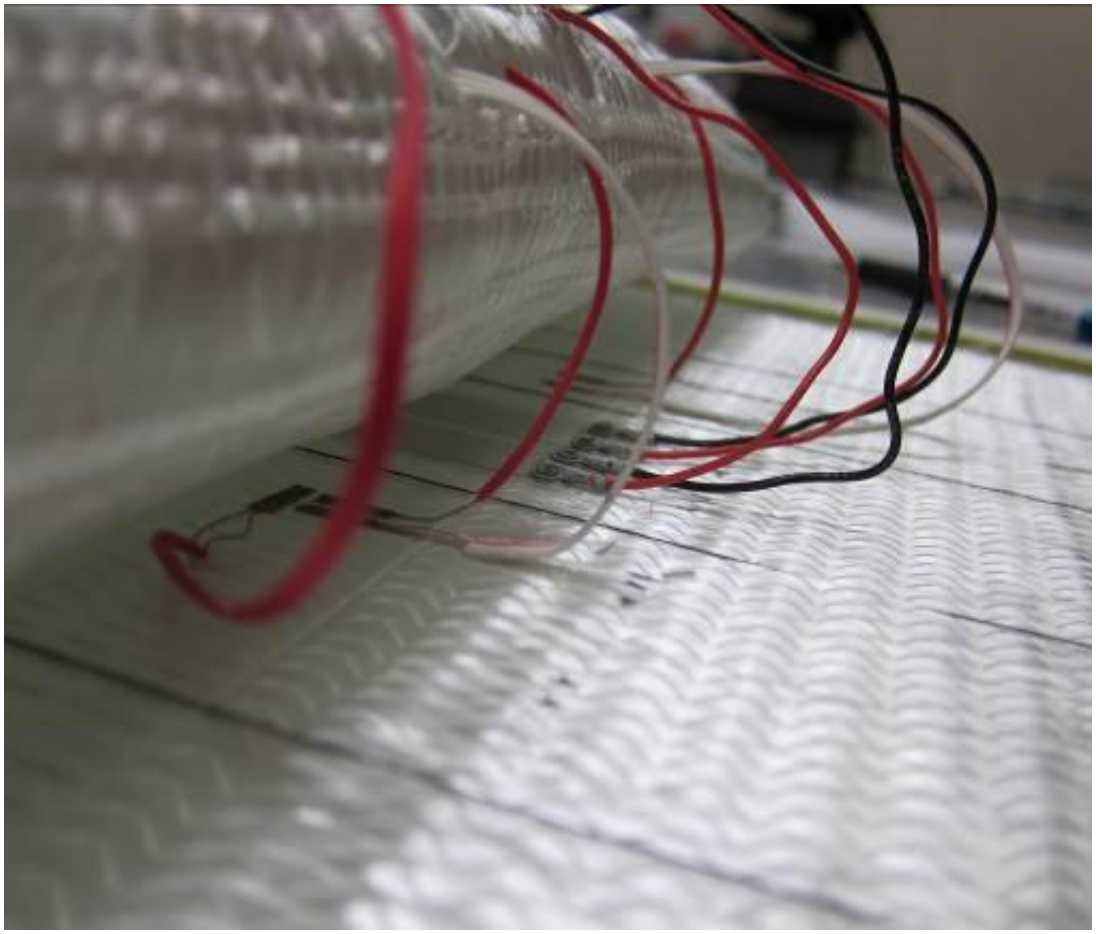

Figure 38. The lead wires being weaved through the tows of the fiber glass

The fibers were then patted down to ensure that the wires were not folded over on themselves, and to make sure that everything was aligned correctly. All 8 layers of the fiber glass lain up with the fibers emerging between the tows is shown in Figure 39.

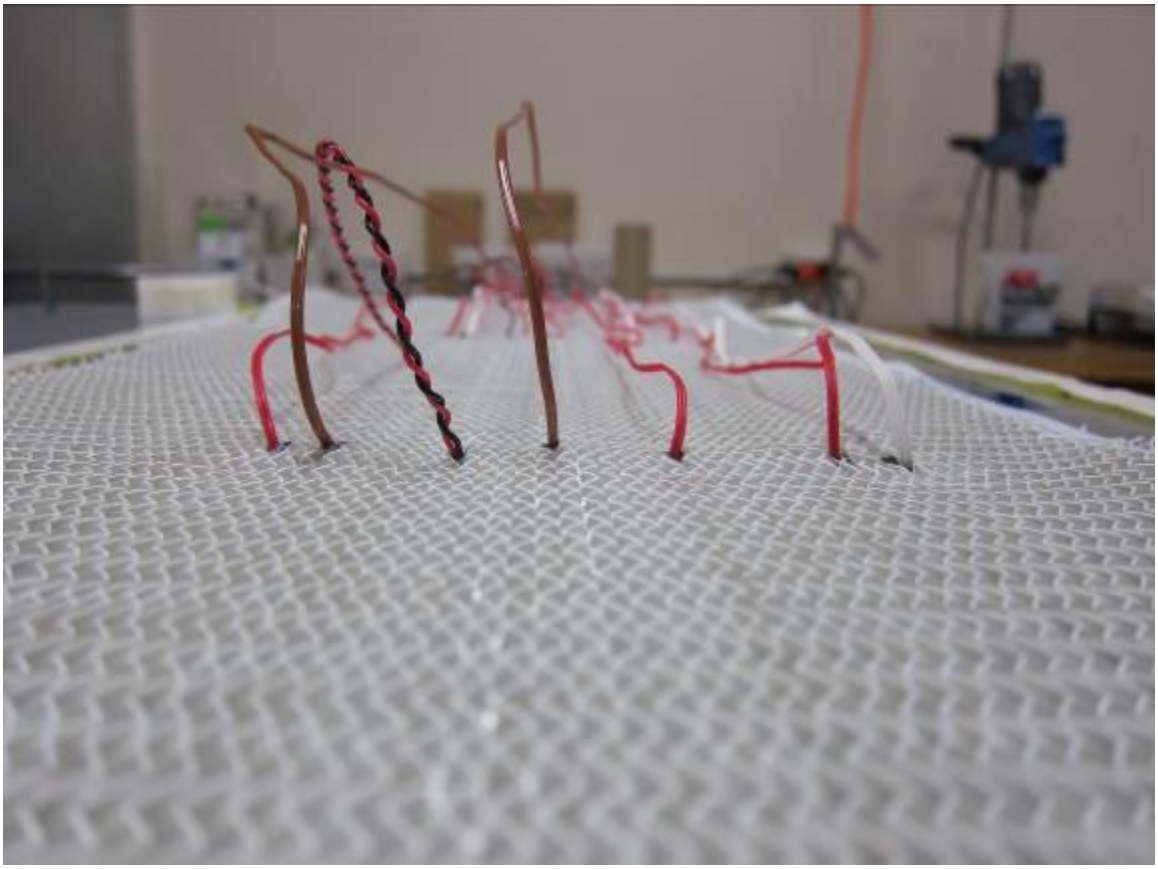

Figure 39. The lead wires coming out through the tows of the fiber glass

Another sheet of peel ply was lain down, followed by one sheet of flow media to help create a more controllable flow front to ensure full saturation of the fibers. A small slit was cut in the peel ply, along with a large rectangular area in the flow media to protect the lead wires when these components were removed after the curing of the resin. Whatever areas are not covered with peel ply, a resin rich, glossy area will be left behind. This is why such a small area is cut away from the peel ply so as to create as uniform of a part as possible.

Since a concurrent project involves measuring the strains and temperatures of the composite while curing, it is essential to have access to the wires. This is a non-trivial

issue, as the VARTM process needs to have the entire composite plate under a vacuum, and any leak will allow air into the part which results in porosity. In order to keep the wires out of the epoxy, several small cuts were made in the top of the vacuum bag for the wires, before it was adhered to the aluminum plate as demonstrated in Figure 40.

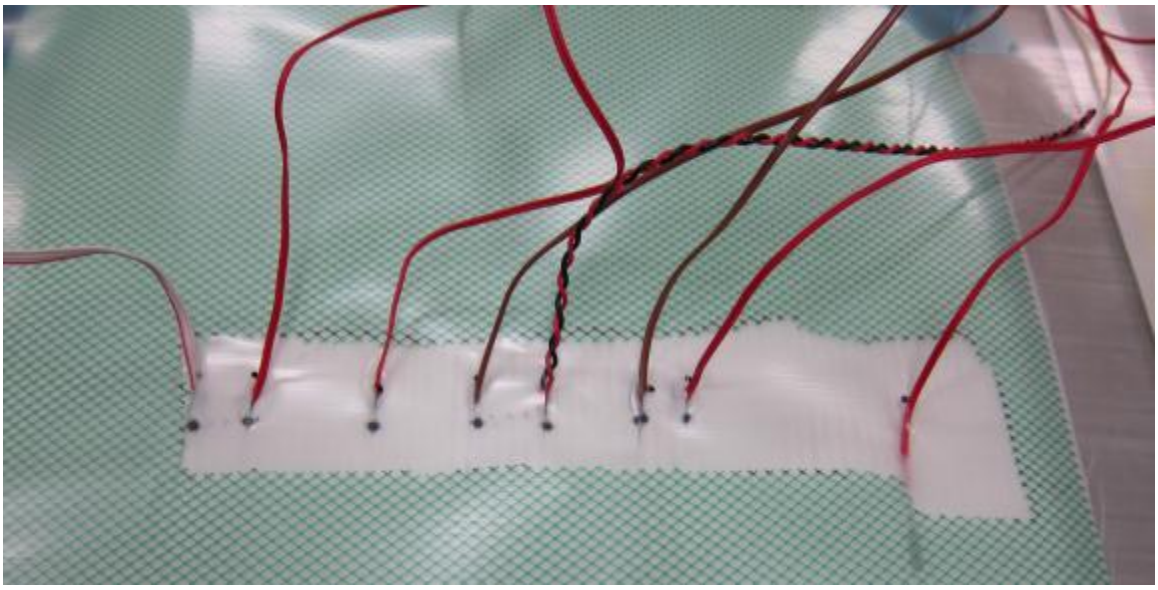

Figure 40. The lead wires of the sensors coming through the fibers, peel ply, flow media, and vacuum bag

To prevent an air leak from ruining the plate, a smaller vacuum bag was placed over the wires, and the wires were run through the thin layer of Tacky Tape in a process known as double bagging. To create a good seal around the wires, a double layer of the Tacky Tape was used. The first layer was lain down around the holes in the vacuum bag, then the lead wires were fed across the tape, and another layer of tape was placed on top of this, and worked around the wires until a good seal was achieved as illustrated in Figure 41.

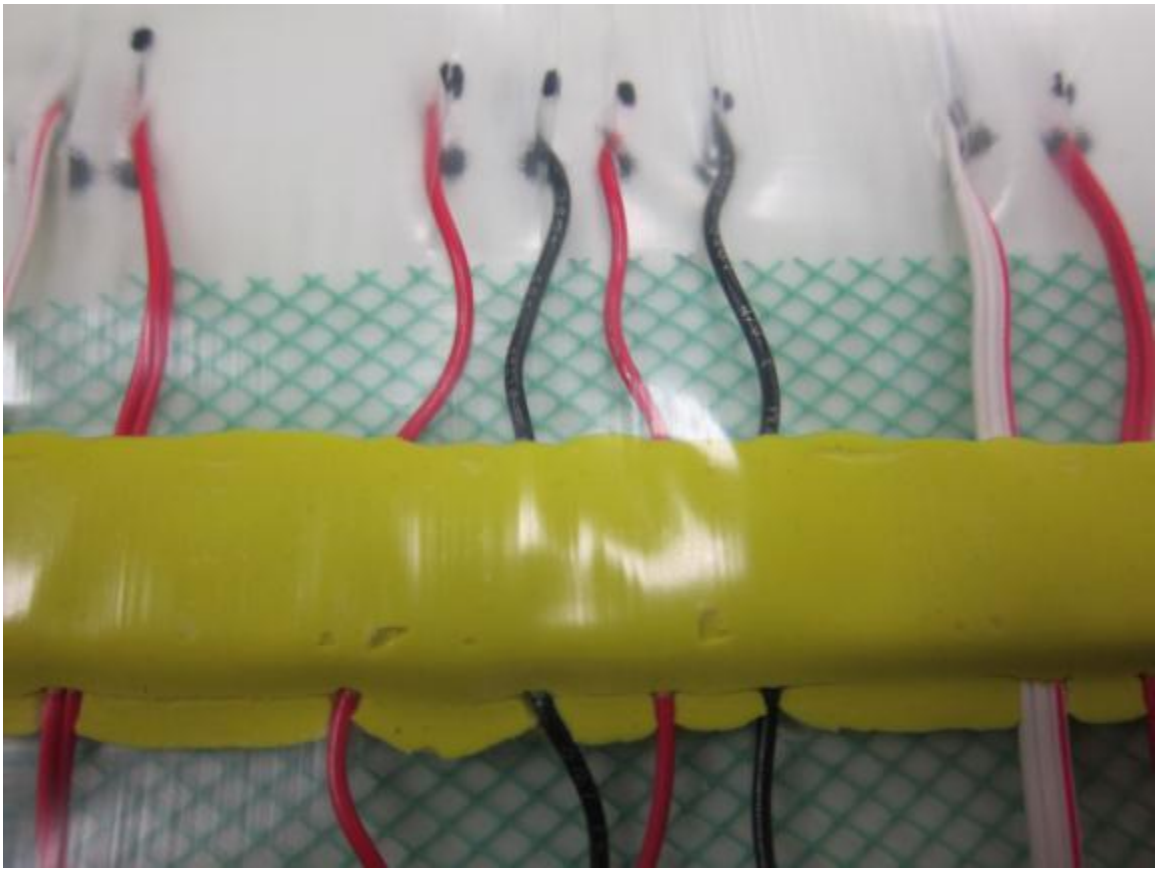

Figure 41. The lead wires sealed between layers of tacky tape to create an airtight seal.

The plate after the injection side was sealed off, and a vacuum of 25.4 inHg was pulled on the whole system is shown in Figure 42. Perfectly sealed, this should hold the vacuum, so this setup was left overnight to ensure that there were no air leaks.

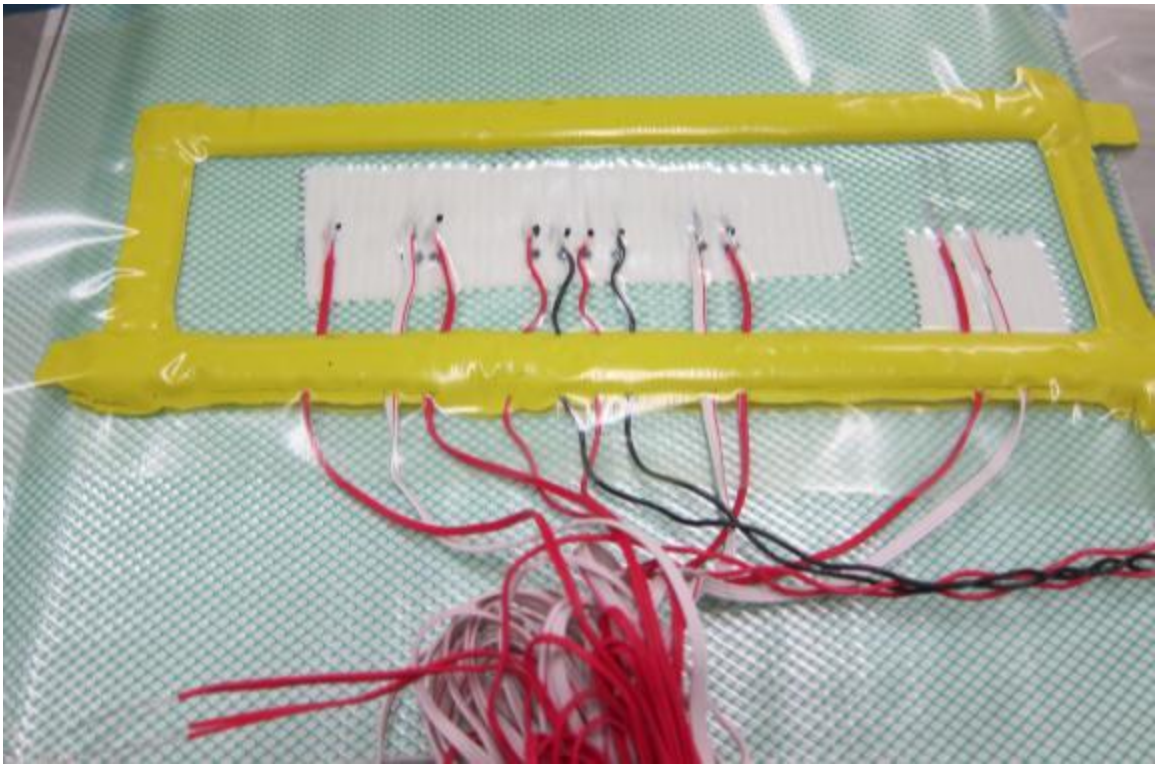

Figure 42. The double bagged area held under a vacuum

If the plate holds the vacuum overnight, the plate is than ready to be infused with resin. The injection tube is placed into the resin, the vacuum pump is turned on, and the clamp on the vacuum side is released. When ready, the clamp sealing off the injection port is slowly opened using an Allen wrench until the resin starts to flow.

The flow is cut off once the resin reaches the vacuum port and starts to drip into the tube. The clamp is than applied to the vacuum side to once again to seal off the system. The plate is then left to cure at room temperature for approximately 24 hours, followed by a 12 hour elevated temperature cure in an oven.

It should be noted that the Gurit Prime resin has a strong exothermic reaction. The heat created will eventually melt the tubing and resin bucket so the injection process

should be done at a reasonable rate so as to avoid the tube melting before the vacuum is sealed off as this will allow air to get into the system and corrupt the plate.

Complications from Embedded Sensors

By embedding a senor into the composite material, the homogeneity of the material is disrupted. However, this issue was addressed in previous work, and the effects on the mechanical properties of the material were not deemed detrimental. However, during the manufacturing of the current plates with embedded sensors showed voids around the location where the lead wires left the composite material.

Another issue that arises is porosity due to the size of the sensors. The resin cannot flow through the sensor, so this disrupts the flow front of the resin as it passes through the material as shown in Figure 43. This can be avoided by using smaller sensors, or by creating an angled flow front to minimize the length of the flow front that is disrupted.

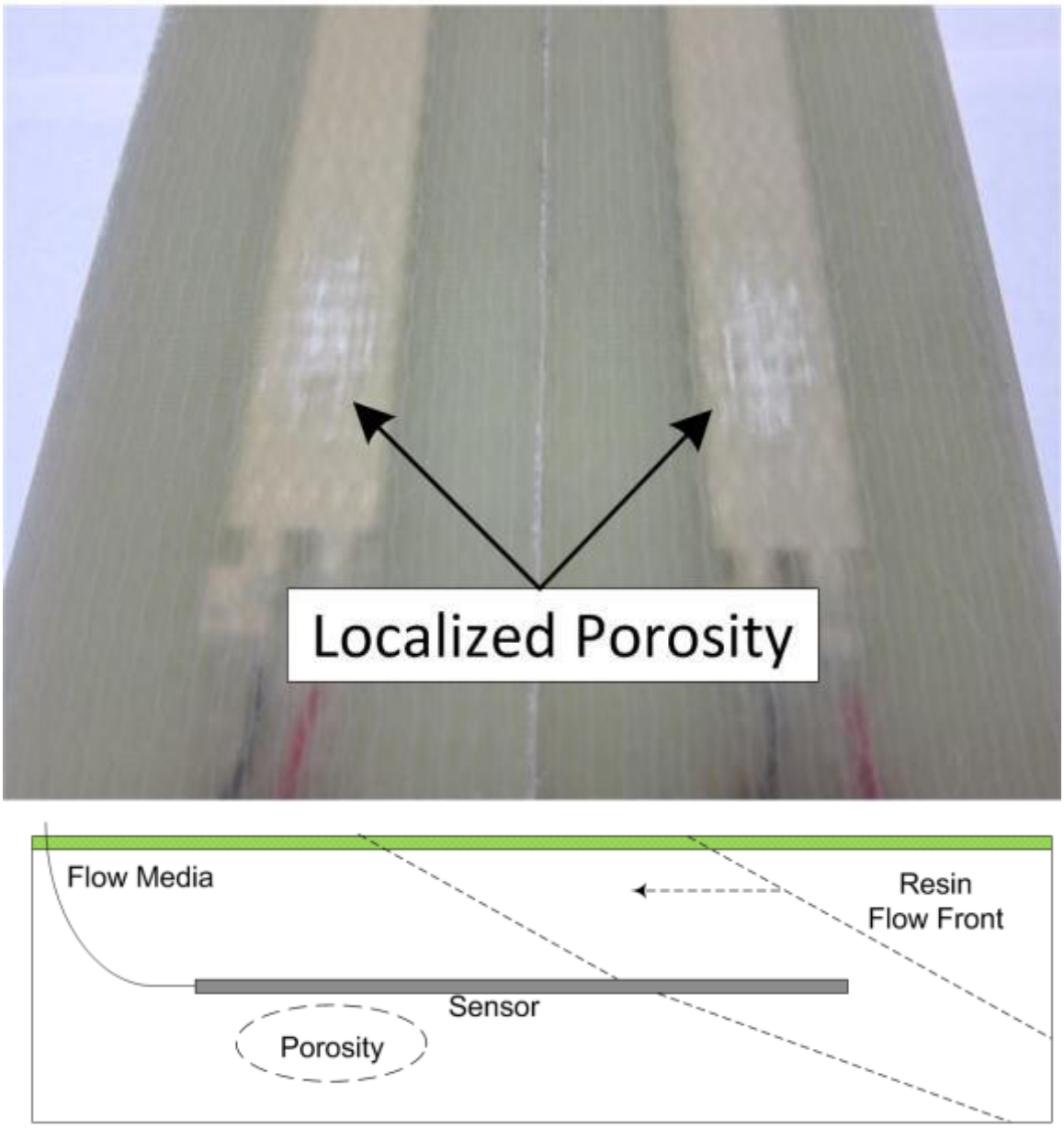

Figure 43. Dry spot caused by presence of sensor

As was mentioned, avoiding porosity is crucial to creating a quality material. Another area where air can get into the composite is around the lead wires. Especially around the thermocouple wires which are sometimes Teflon coated. If the lead wire is braided rather than a solid wire, there is also the possibility that air can enter through the

inside of the insulation. Liberal use of the tacky tape around these areas is recommended to try to seal any possible source of leak. This is the reason for allowing the plate to sit overnight with a vacuum held to make sure that all possible areas of leakage are sealed. The average timetable for laying up the plate with embedded sensors is shown in Table 9.

Table 9. The major steps of laying up a composite plate with embedded sensors

DAY	PROCEDURE
1	Cut and prepare materials
	Layup sheets of fiber to sensor location
	Apply sensors using adhesive
2	Layup additional sheets of fiber
	Weave lead wires through these sheets
	Complete layup process
	Pull vacuum
3	Check for leaks in vacuum bag
	Mix resin and inject plate
4	Remove plate from aluminum mold
	Place in oven for post cure
5	Remove plate from oven Cut samples

TESTING & EXPERIMENTAL RESULTS

General Analytical Solution

Since only uni-directional layups were used, and simple tensile tests were performed, the rule of mixtures solution for the material modulus was sufficient for the analysis. From the rule of mixtures (Equation 1), the value for E_1 was found to be roughly 45 GPa. This estimate was performed under the assumption of a 60% fiber volume fraction, and ignoring any effects of the sensor embedment. The typical sample geometry tested, had a total of 8 layers which led to a thickness of approximately 5 mm, and a width of either 25 mm or 50 mm, so as to fit in the available grips.

To predict the strain in the composite material, Hooke's law (Equation 2) was used in conjunction with the previously found modulus of elasticity to calculate the predicted strain for a given stress.

Since the typical maximum load applied to the specimen was 5 kN, the stress was calculated from the known cross sectional area of the sample, and then plugged into Hooke's law. Therefore, for the sample being tested, the expected strain was 1020 με.

MFSGs

The metal foil strain gages were tested under several different loading conditions to ensure that the response seen from the circuit was properly mimicking the thermal and mechanical loading being applied. As described in the test plan found in Table 2, testing was initially conducted with the gages adhered to the surface of aluminum stock to ensure

that the circuit was working correctly and that the gage was showing the expected response. Then the tests were repeated with the sensors adhered to the surface of the uni-directional composites, as well as embedded in the composites. These tests were first performed under a tensile load, and then redone for a thermal loading condition, and finally a combined loading scenario.

Since photographs of the circuit can sometimes be misleading and confusing to follow, the circuit was lain out in Visio to make it easier to understand. The Wheatstone bridge circuit that has previously been discussed was wired as shown in Figure 44. This diagram shows the breadboard circuit that was designed for use in all of the experimentation, alongside the standard diagram of the circuit. The resistors shown in the diagram are all 120 Ω, to correspond with the 120 Ω gages.

Tensile Testing

Measuring the strain from a tensile load is what MFSGs were designed for. Therefore, the tensile tests were performed to ensure that the gages were working correctly. An Instron 5882 was used to perform all of the tensile testing. The sample was loaded into the grips, and a displacement controlled tension test was performed at a rate of 1 mm/min for most of the MFSG tests up to a maximum load of 5 kN. As illustrated in Figure 45, there are several pieces of equipment required for all of the tensile tests.

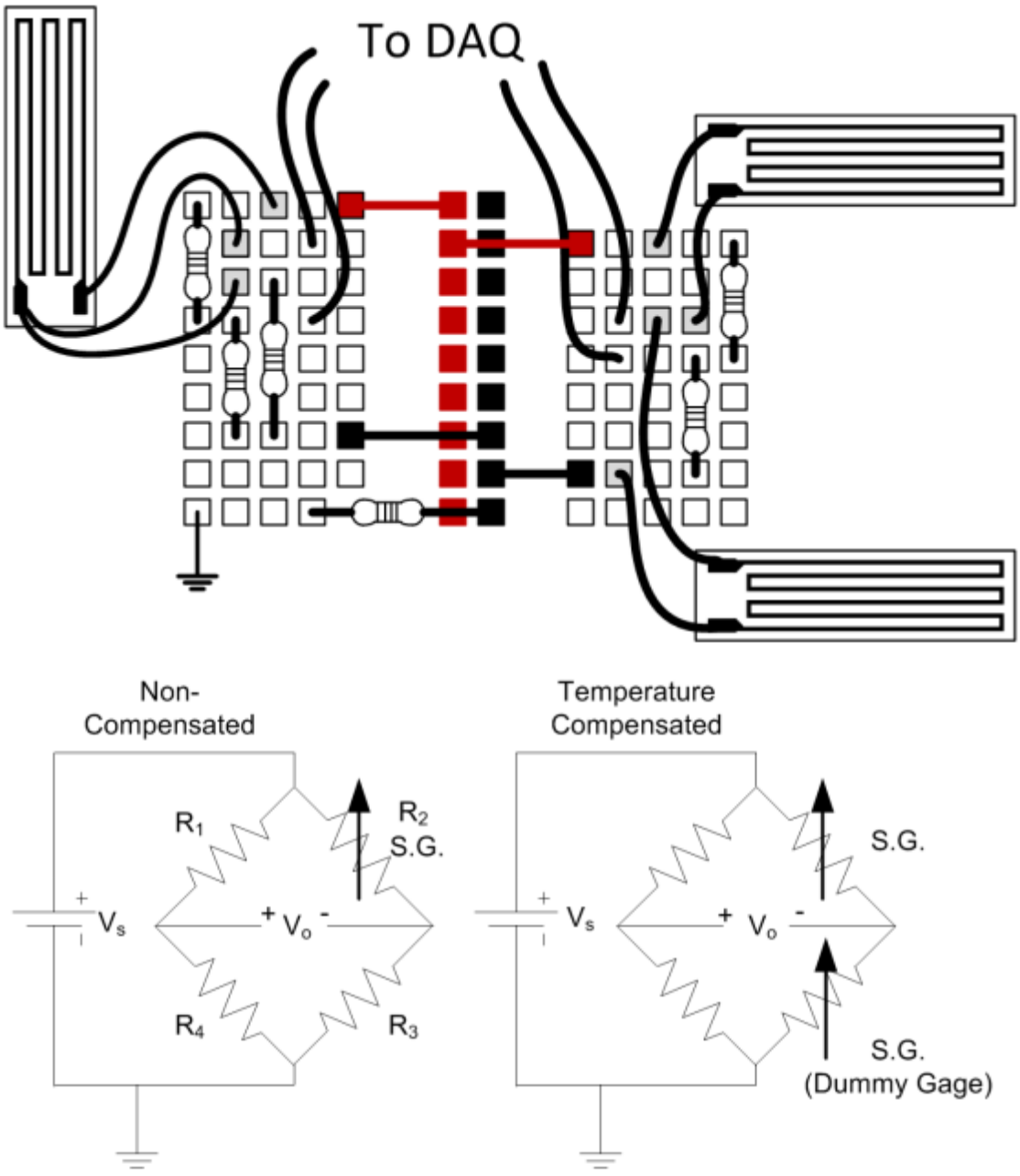

Figure 44. Wheatstone bridge as wired on a breadboard along with the correspond circuit diagram

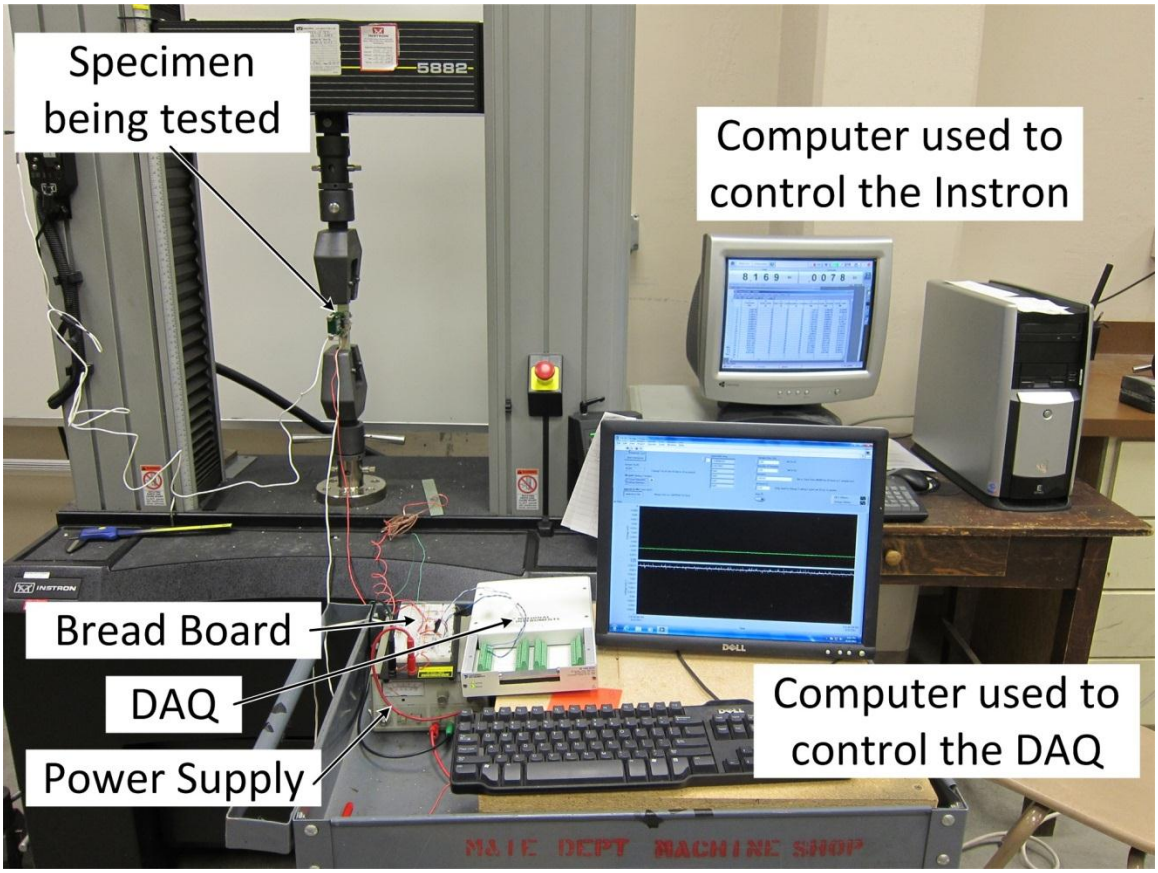

Figure 45. The testing setup for all of the tensile tests along with all of the important components

The test plan was followed in that the test was originally performed on an aluminum bar, followed by the surface mounted gages, and finally the embedded gages. Each of these steps was performed to arrive at the final testing of the embedded gages with an extensometer. Therefore, only the results from the final set of tensile tests are presented. The extensometer mounted onto the specimen while loaded in the Instron's grips is shown in Figure 46. The extensometer works much like the MFSGs through the use of a Wheatstone bridge, except for that it has all of its circuitry built in, and it connects directly to the Instron through a 25 pin serial port, where all of the calculations are performed before displaying the percent strain. The use of an extensometer is very

important to accurate strain measurements, as the cross head displacement of the Instron usually returns an unreliable value, due to the possible strain in all of the linkages and other components that hold the specimen.

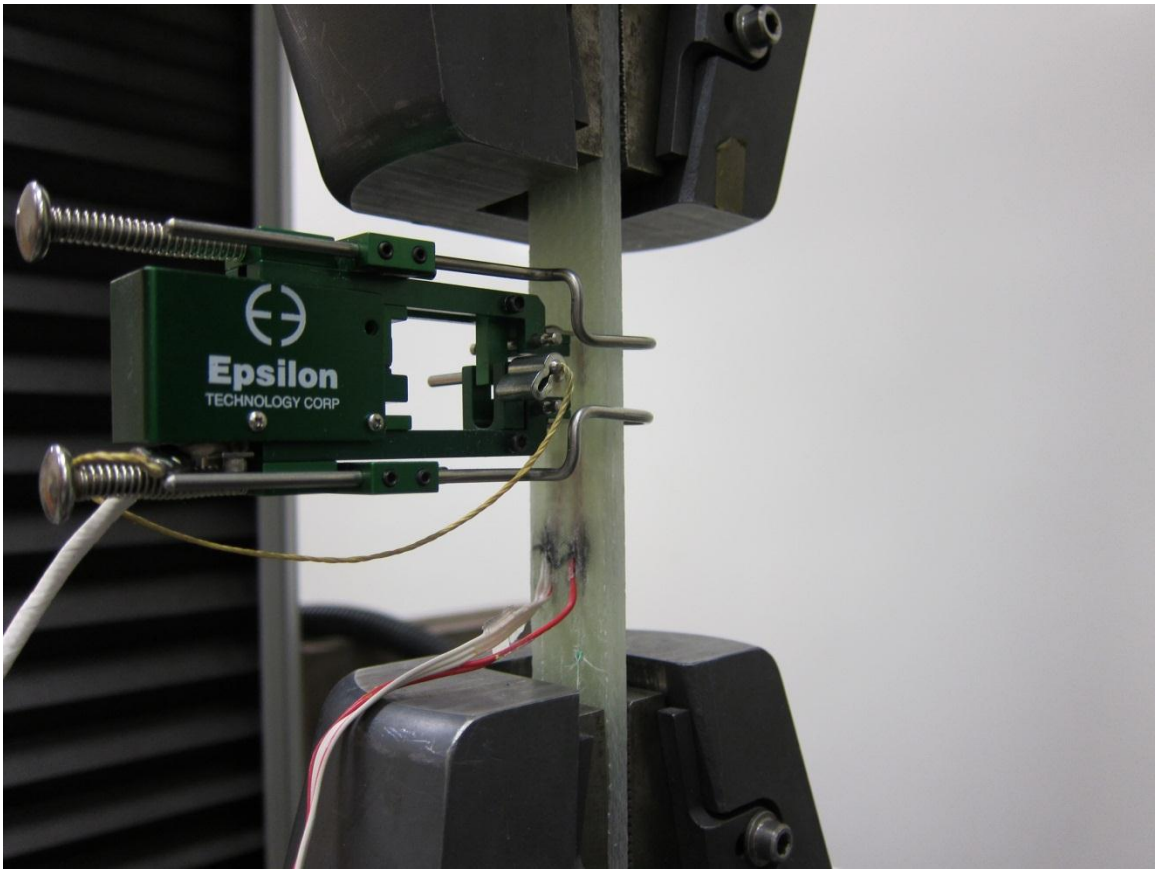

Figure 46. Tensile test specimen with embedded 3-wire and 2-wire strain gages along with an extensometer for correlation

As shown in Figure 47, the stress strain curve of the composite sample was plotted and an experimental modulus of 51 GPa was found. The stress was calculated from the load that was obtained from the load cell of the Instron, and the strain was monitored using the external extensometer.

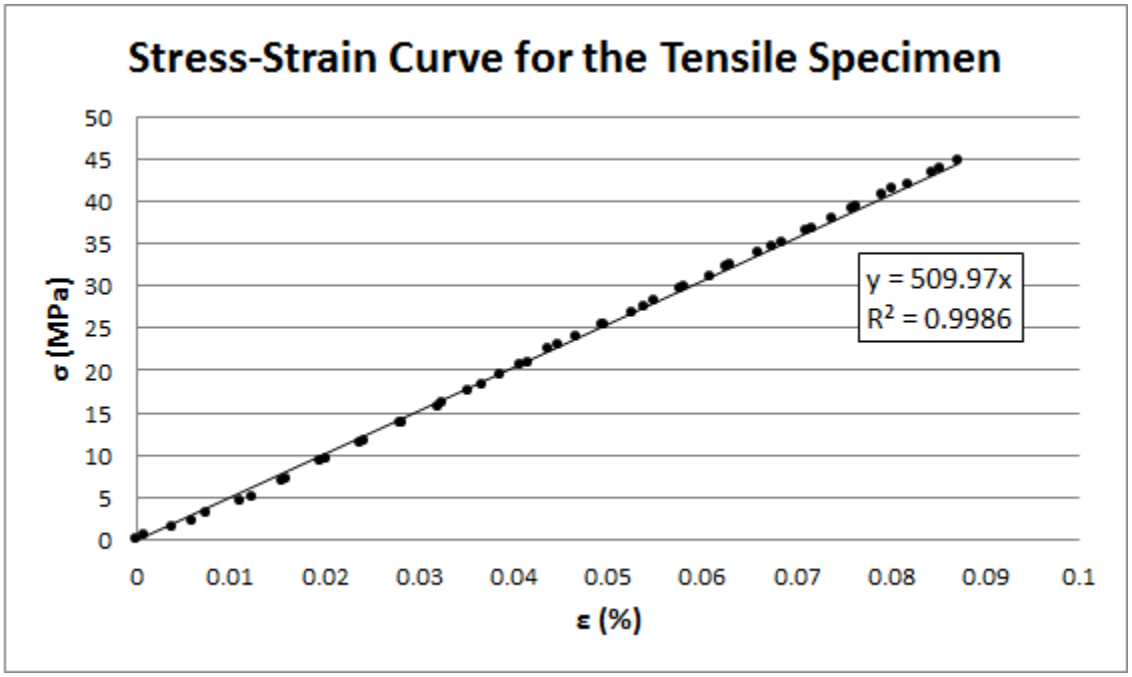

Figure 47. The average stress-strain curve of the composite specimen. The maximum strain was 875 με at 45 MPa

As illustrated in Figure 48, the correlation between the strain measured by the strain gages and the strains measured by the extensometer is quite good. The data utilized in the graph was taken as the same time as the stress strain curve in Figure 47. After the conversion, the 3-wire strain gage in the quarter bridge showed a maximum strain of 868 με, where the 2-wire MFSG in the half bridge configuration showed a maximum value of 800 με.

The comparison of the maximum strain values measured by each of the gages to the results from the extensometer is shown in Table 10. The reasons for any discrepancy could come from misalignment of the gage, possible localized porosity that could alter the stiffness of the material, or calibration issues of the load cell or extensometer.

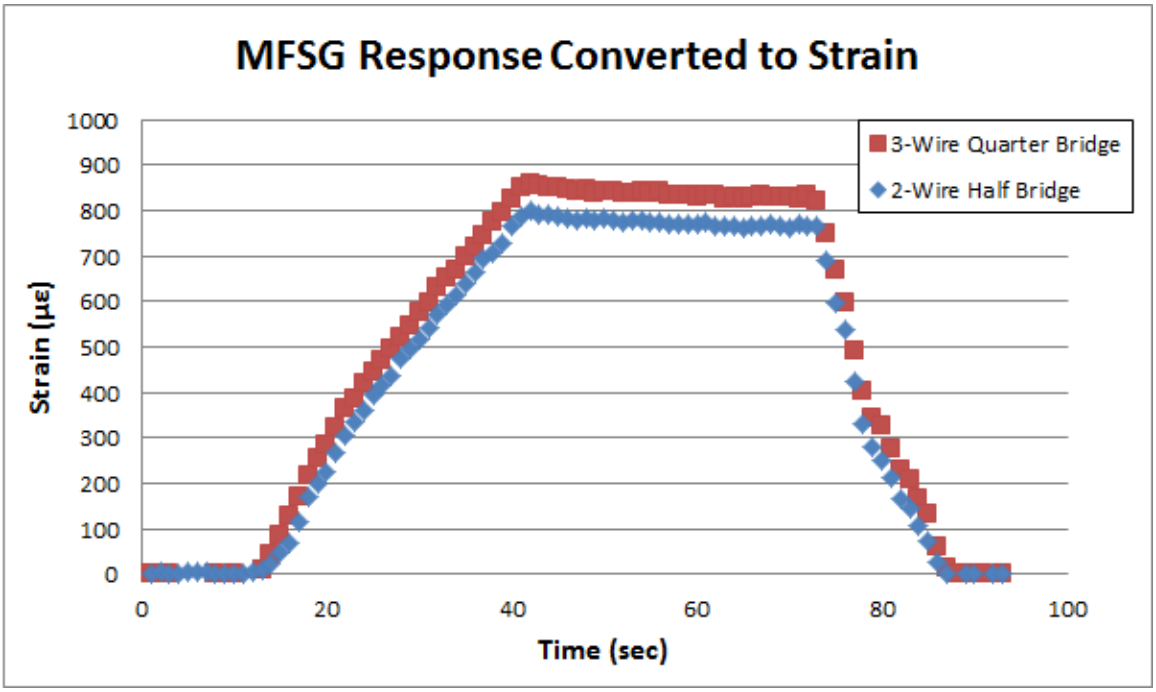

Figure 48. Measured strain from MFSG from a quarter bridge and half bridge circuit

Table 10. Comparison of the various measurements of strain compared to that of the extensometer

Measurement	Value	% diff
Extensometer	875	-
Calculated	1020	16.57
2-wire HB	800	8.57
3-wire QB	868	0.8

Heating

Several heating tests were performed to ensure that the sensors were reacting as expected to changes in temperature. An Instron oven was used for all of the heating and is shown in Figure 49.

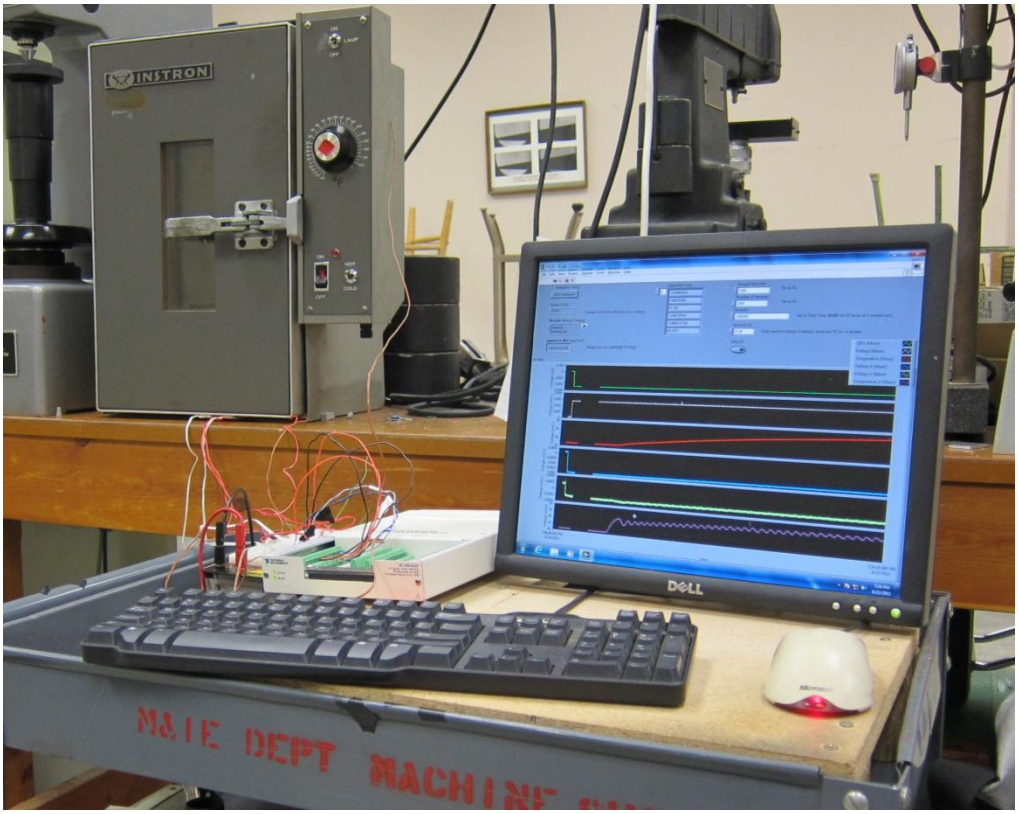

Figure 49. The testing setup for all of the heating tests

After performing all of the experiments from the heating portion of the test plan, what appeared to be residual strain from heating was observed in the data. Several hypotheses were developed for what might be causing this issue, ranging from additional curing to resistive heating caused by the gages.

After investigating the results from the embedding MFSG heating tests, an initial change in resistance of the MFSG was shown by a change in the output voltage. However, as indicated by the embedded thermocouple, the internal temperature of the composite sample had not yet begun to change. Therefore, it was hypothesized that the change in temperature of the lead wires was skewing the results. The 3-wire strain gage is designed to eliminate this issue, but was not initially considered as they are typically

used in cases where very long lead wires are needed, and only a short section of wire was being heated. Therefore, the 3-wire strain gage configuration was adopted for the quarter bridge testing, and the series of experiments was repeated. One of the tests performed to demonstrate the need for the 3-wire strain gages was the second step of the test plan which involved two surface mounted strain gages in a quarter bridge configuration, one with each type of gage. These were heated inside an oven up to 75 C as shown in Figure 50. The 3-wire MFSG followed the temperature profile of the oven quite well, whereas the response from the 2-wire MFSG showed a similar initial response, but once the oven was turned off, the signal did not follow the cooling trend. It was also noted that the heating of the lead wires causes a negative response in the 2-wire MFSG. This confirmed the need for the 3-wire MFSG for accurate thermal measurements utilizing the strain gage configuration.

To ensure that the embedment process did not affect the response of the gages, the test was repeated with the embedded 3-wire MFSG in a quarter bridge configuration as prescribed by the test plan. The oven was heated to 50 C, and the measured strain was compared to the temperature response from an embedded thermocouple. As illustrated in Figure 51, there is more noise in the system, yet it still follows the correct trend.

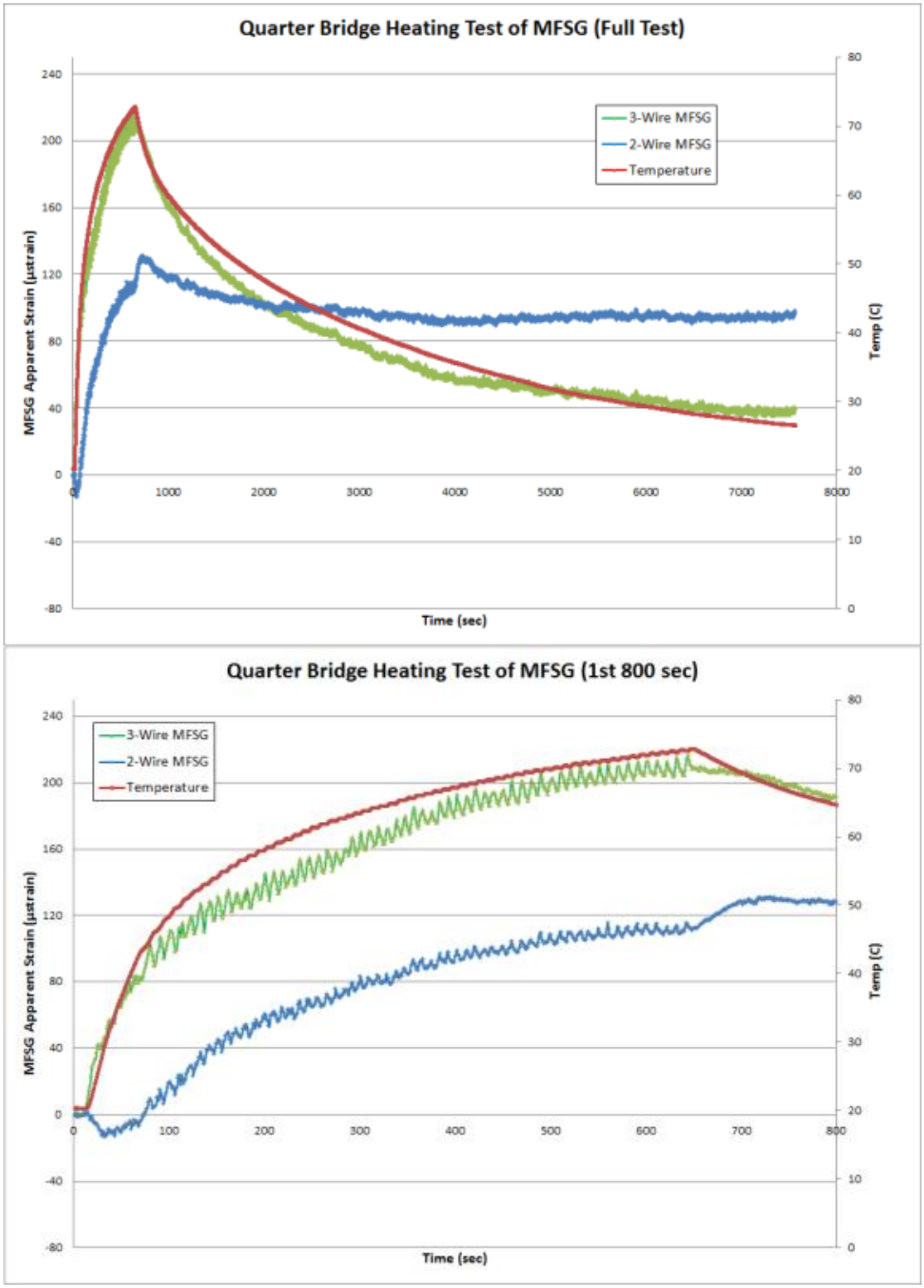

Figure 50. Heating test of 3-wire and 2-wire surface mounted MFSGs compared to the temperature of the oven

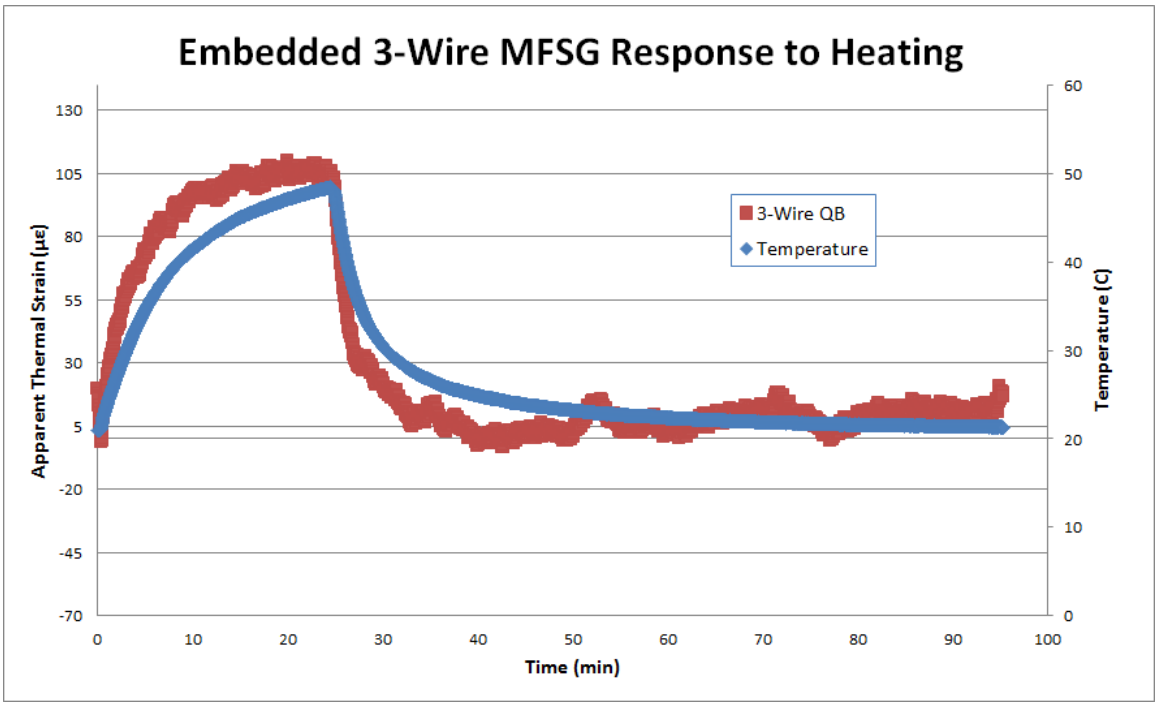

Figure 51. Heating test of an embedded 3-wire MFSG

Combined Testing (Heating and Tensile)

To prove that it was possible to separate the thermal and mechanical responses from one other using only a set of MFSGs, the set of one quarter bridge and one half bridge were both heated in the oven up to 50 C, and then covered in insulation to minimize heat loss, and placed in the Instron. A displacement controlled tensile test with a rate of 0.1 mm/min up to 1 kN was then performed. The reduction in maximum values of the rate and load were to keep the thermal and mechanical responses on a similar scale for easier viewing. The response from the two different configurations is shown in Figure 52. As expected, the half bridge is not affected by the change in temperature.

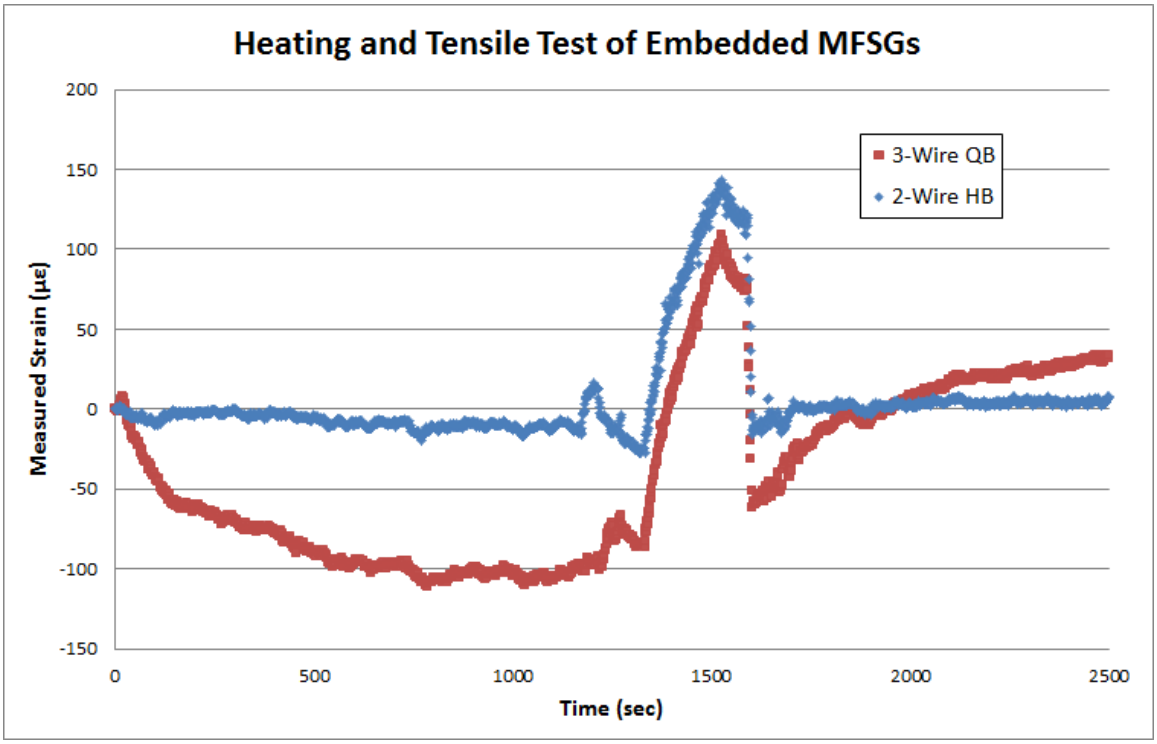

Figure 52. Combined heating and tensile test of embedded MFSGs

The apparent thermal strain is the difference between the quarter bridge and half bridge. The difference between the two measurements, compared to an embedded thermocouple's temperature reading is shown in Figure 53.

To relate the output signal to the applied loading condition, the sensitivity of the MFSG was calculated for both the thermal and mechanical load as shown in Figure 54. The data was taken from individual testing results, and only a sample of the data during the loading phase was utilized. The calculated sensitivities, along with the mean value and standard deviations, are shown in Table 11, and are used in conjunction with Equations 10 & 11.

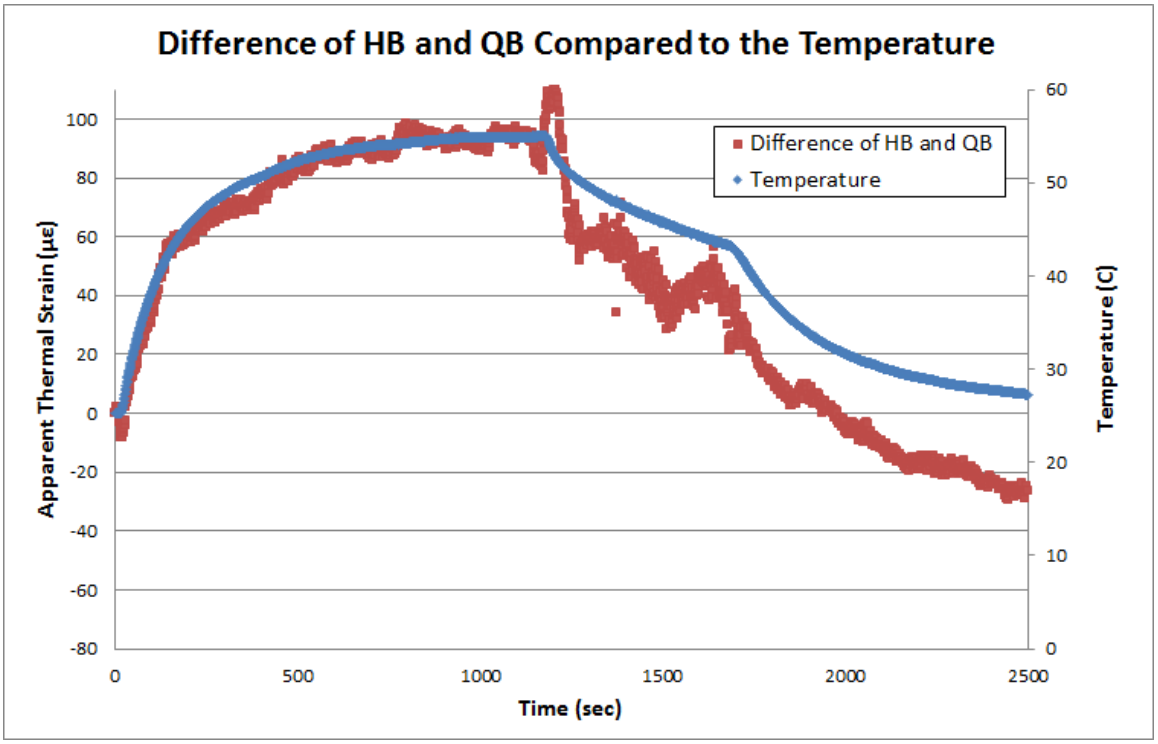

Figure 53. The calculated apparent thermal strain from a heating and tension test

$$\varepsilon_{mech} = S_{mech} * V_{QB} \quad \text{Equation 10}$$

$$T = S_{therm} * V_{QB-HB} \quad \text{Equation 11}$$

Where

$S_{mech} = mechanical\ sensitivity$

$S_{therm} = thermal\ sensitivity$

$V_{QB} = Measured\ voltage\ from\ QB$
$normalized\ by\ the\ source\ voltage$

$V_{QB-HB} = Measured\ differential\ voltage\ from\ QB$
$and\ HB\ normalized\ by\ the\ source\ voltage$

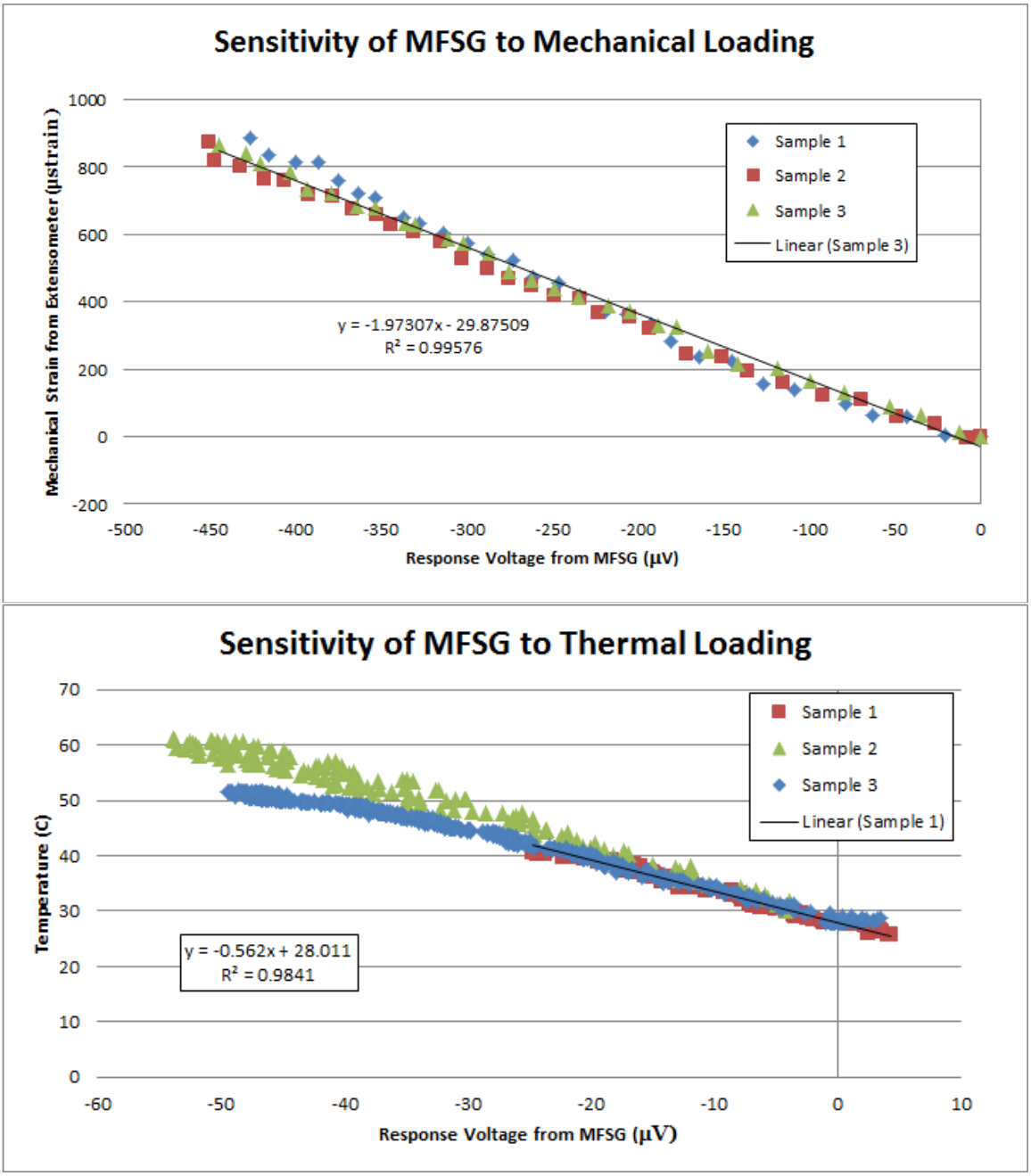

Figure 54. The sensitivity of the MFSGs to applied strain and temperature fields

Table 11. Sensitivity of MFSGs

	Mechanical		*Thermal*	
Sample 1	-1.937994		-0.562	
Sample 2	-2.177783	με/(μV/V)	-0.47128	°C/(μV/V)
Sample 3	-1.973069		-0.59418	
Mean	-2.0296	με/(μV/V)	-0.5425	°C/(μV/V)
Standard Deviation	0.1295		0.0637	
Standard Deviation (% of mean)	6.38	%	11.75	%

PVDF Films

Since the response is time dependent, several tests were performed to demonstrate this, and show the possibilities of these sensors. Again, it was desirable to be able to completely separate the mechanical response from the thermal response, so that it was clear what was affecting the gage.

A set of tests were performed to try and do this through advanced filters in an attempt to recreate some of the research done at the University of Minho in Portugal [22]. It was hypothesized that the frequency response from mechanical loading was different from the frequency response of heating the sample. Several tests were performed using Fourier Transforms to try to quantify the frequency response of the PVDF film due to either heating or mechanical loading. However, the results found did not correlate with those presented, and the approach was abandoned.

The charge amplifier circuit that was built and tested for a single PVDF film sensor along with the circuit diagram is illustrated in Figure 55. The dual gage configuration is made by adding another PVDF film in the same location as the PVDF film that is already wired in, but with the lead wires reversed.

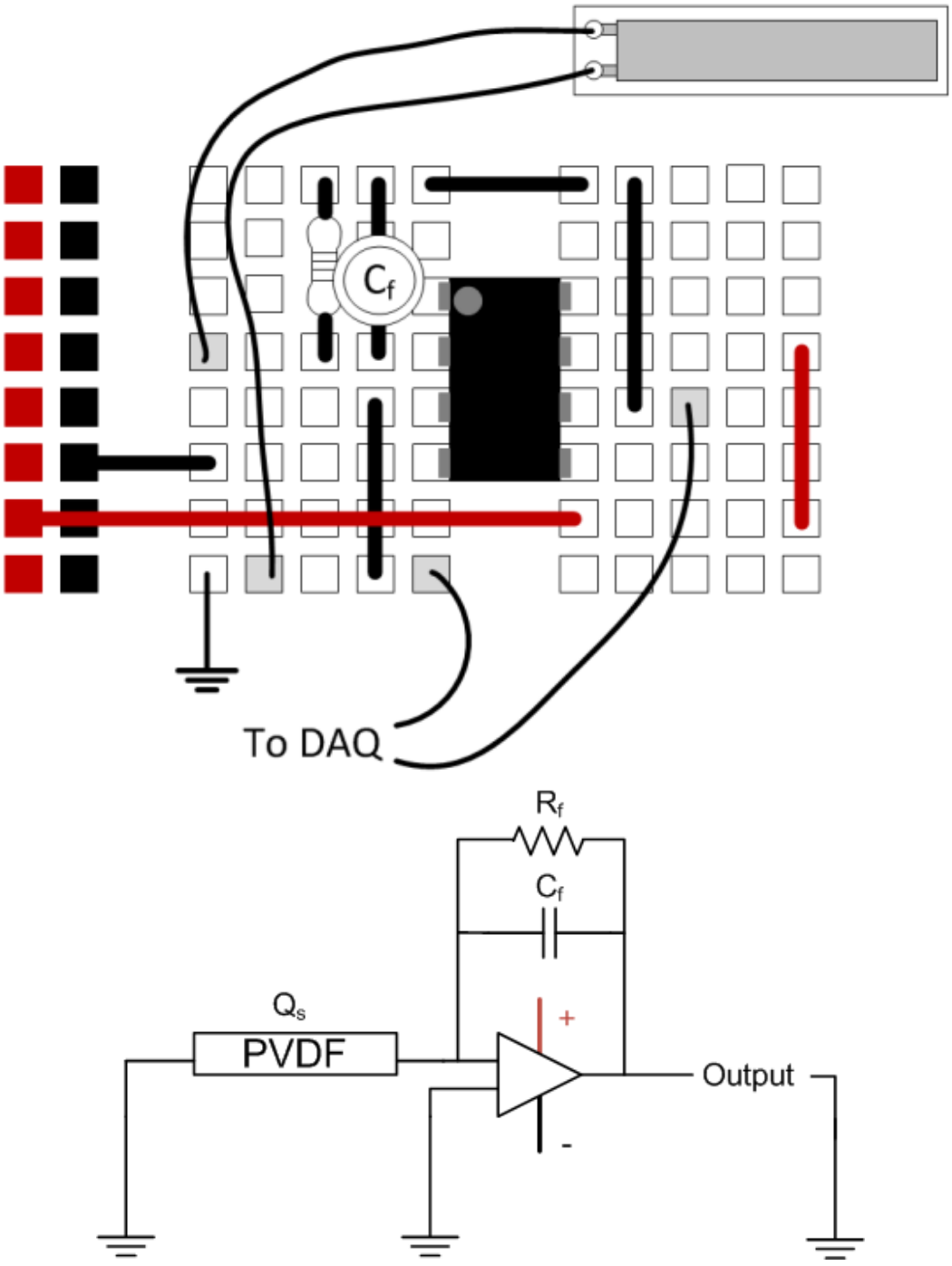

Figure 55. Charge amplifier circuit as built on the breadboard along with its circuit diagram

To investigate the effects of varying the time constant, several combinations of feedback resistors and capacitors were used and a simple tensile test was performed with

the same parameters. This was the first experiment done to determine which set of components to proceed with for the proceeding tests. The experiment was conducted using the Instron 5882. A displacement controlled tensile test was done at a rate of 1 mm/min to a maximum load of 10 kN. The combination of resistors and capacitors is shown in Table 12.

Table 12. Capacitance and resistance values used in the charge amplifier circuit

Test #	Resistor (MΩ)	Capacitor (μF)	Time Constant (sec)
1	2	1	2
2	5	1	5
3	10	1	10
4	10	0.1	1
5	20	0.1	2
6	50	0.1	5

The time constant is defined as the time required for the signal to decay to 36.8% of its original value [18]. Therefore, as illustrated in Figure 56, the higher the time constant, the longer it takes for the signal to reach its maximum value, or decay back to its null value. All of the PVDF results had a non-zero equilibrium voltage. Therefore, to make it easier to compare the results, the curves were shifted so that their equilibrium value was close to zero. Tests 1-3 are shown in the top part of Figure 56, where tests 4-6 are shown in the bottom part of the figure. It is also clear that the higher the time constant, the larger the amplitude of the response. However, there is also more noise at these higher amplitudes. From Equation 8, the smaller the feedback capacitance, the larger the response from the charge generated on the PVDF film. As expected, by

decreasing the capacitance by a factor of 10, the response amplitude is increased by a factor of 10.

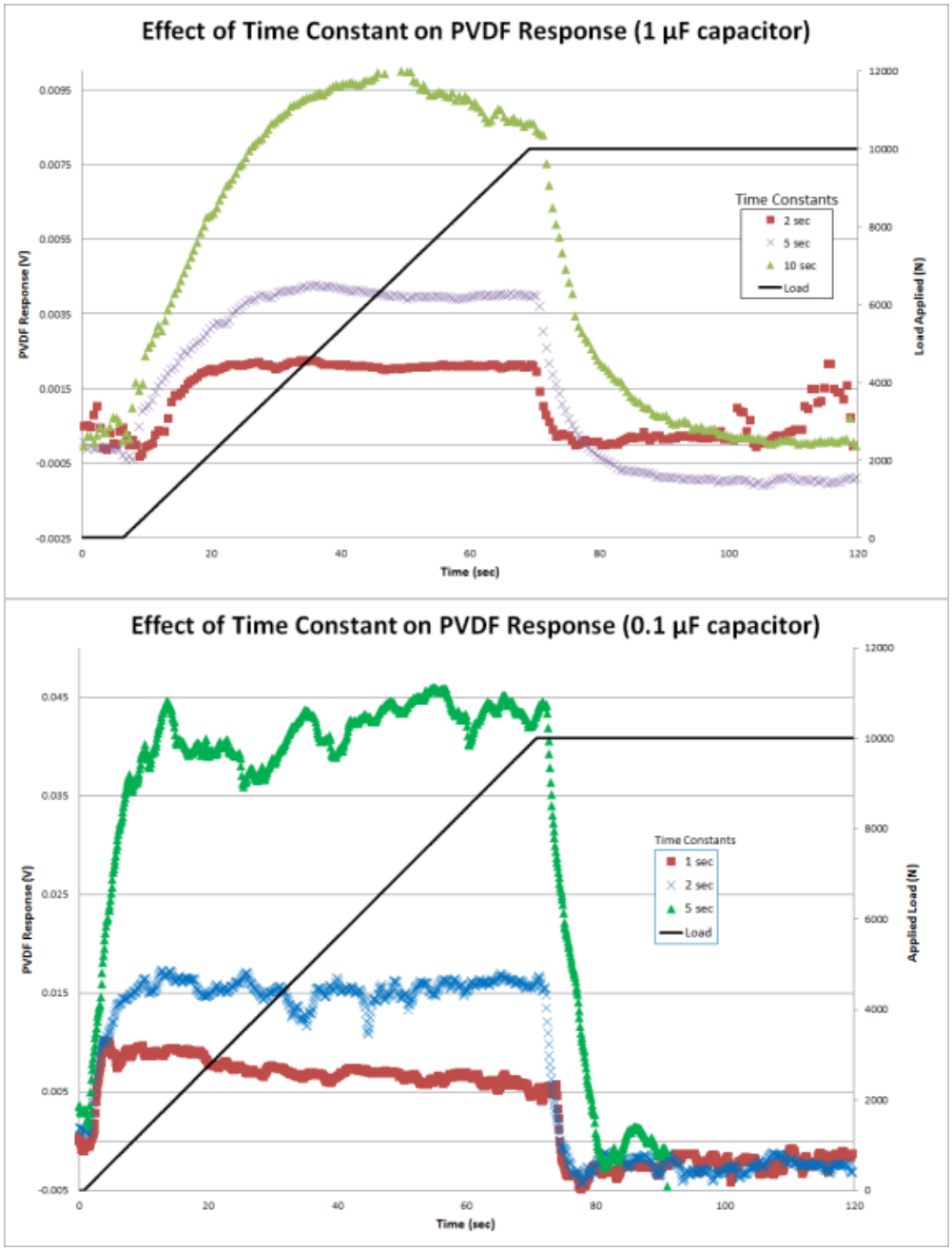

Figure 56. Investigation of the effects of various capacitors and resistors on the output of the charge amplifier circuit

Tensile Loading

The tensile testing was done using the Instron 5882, up to a maximum load of 4500 N. The charge amplifier circuit was setup with a 1 μF capacitor, and a 10 MΩ resistor, which gave a 10 sec time constant. A MFSG was also adhered to the composite sample to have a baseline to compare with. The specimen as loaded in the Instron is shown in Figure 57. As prescribed by the test plan shown in Table 3, the initial tensile testing was performed on an aluminum bar to mitigate any issues of embedding the sensors into the composite material. The aluminum sample was loaded into the Instron and a load controlled test was performed.

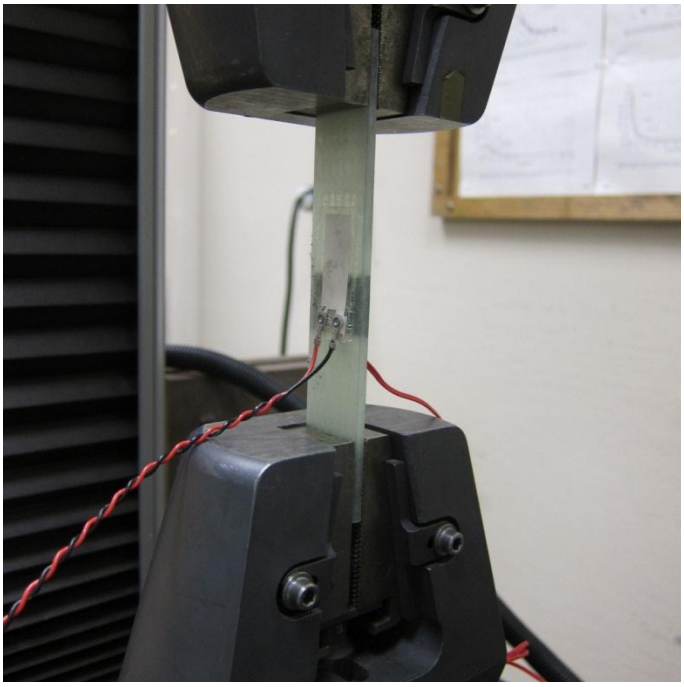

Figure 57. Surface mounted PVDF film undergoing a tensile test

The tensile testing with only the 66 N/s load rate displayed is presented in Figure 58, to demonstrate the various parts of the test. The response of the MFSG matches the

loading curve quite closely. The curve in section 1 corresponds with the constant loading section. It is clear that the curve levels off after a time even while the sample is still being loaded. After the maximum load was reached, it was held constant for one minute at this load, which is shown in section 2 on the graph. The sample was then unloaded at a fairly constant rate for all of the samples (section 3). In section 4, the sample was completely unloaded, but the response of the gage was returning to zero.

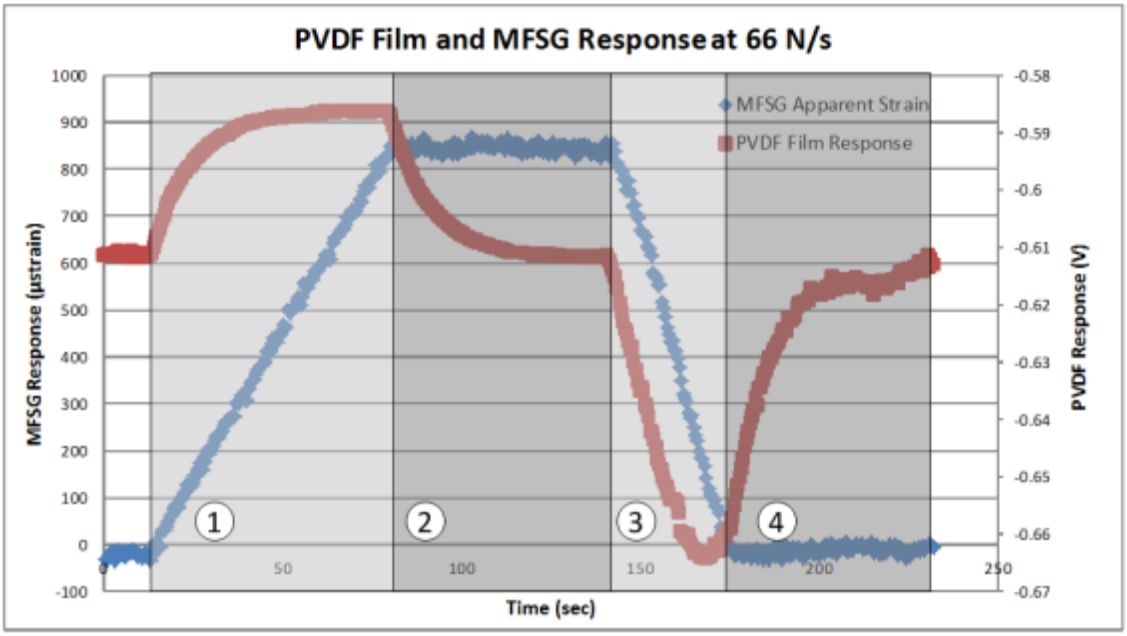

Figure 58. PVDF film response due to tensile loading

The test was repeated with varying load rates from 22 N/s up to 110 N/s to demonstrate the importance of load rate on the PVDF films. All tests were run up to a maximum load of 4500 N. As demonstrated in Figure 59, the higher the load rate, the larger the response of the gage. It can be seen that the samples were all unloaded at a consistent rate, since they all reach approximately the same maximum negative value.

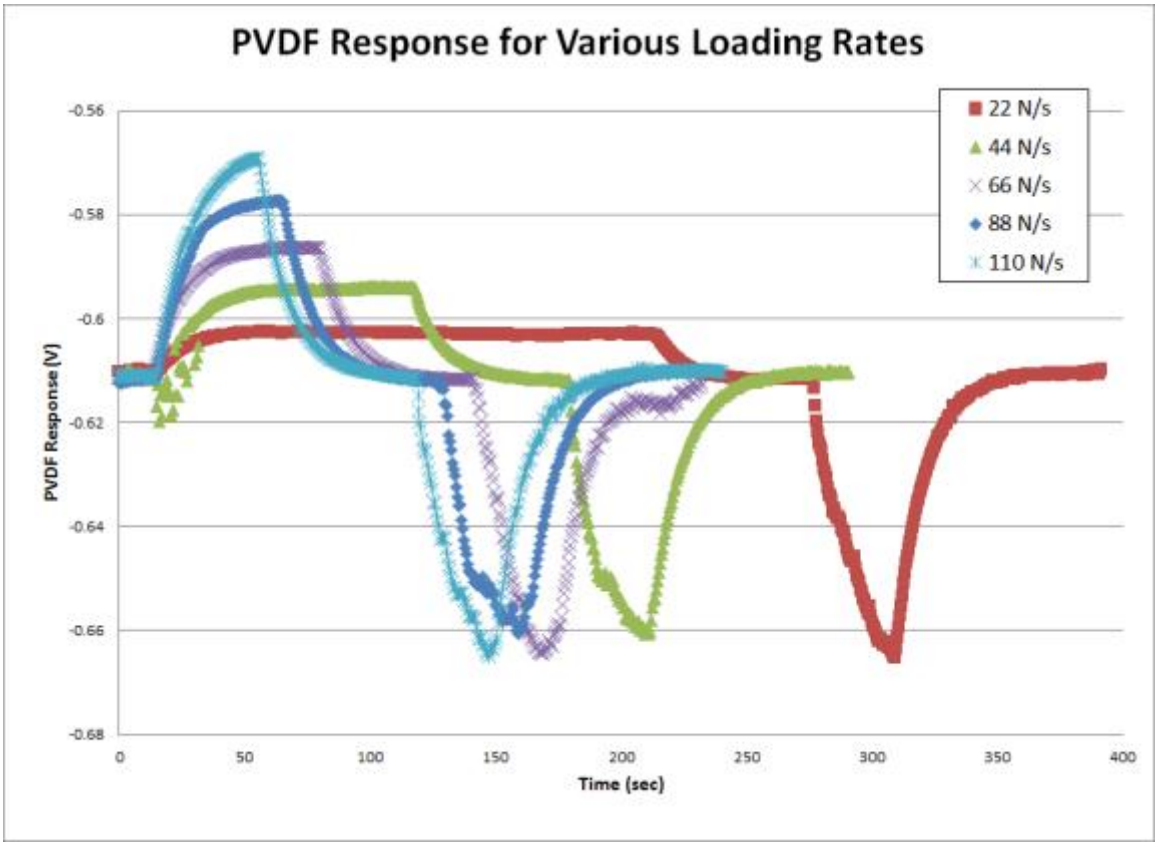

Figure 59. PVDF film response of multiple load rates

Heating

A series of heating tests were performed on the composite samples with embedded and surface mounted PVDF films. The samples were placed in the oven, and heated to an elevated temperature, and then held to watch the response of the gage.

One representative test that was performed looked at the response of the PVDF film that was adhered to the surface of the composite sample. Since the sensor was exposed to the environment, it was more susceptible to the changes in temperature of the oven. The oven used experienced a cyclic heating cycle, and this was well captured by the PVDF film as shown in Figure 60. The oven was set to roughly 47 C, and when turned on, the initial jump in temperature was the greatest (from 22 to 40 C). This jump

registered the largest change in response from the PVDF film. However, after this initial peak value, the response of the gage begins to return to its equilibrium value of approximately -3.42 V.

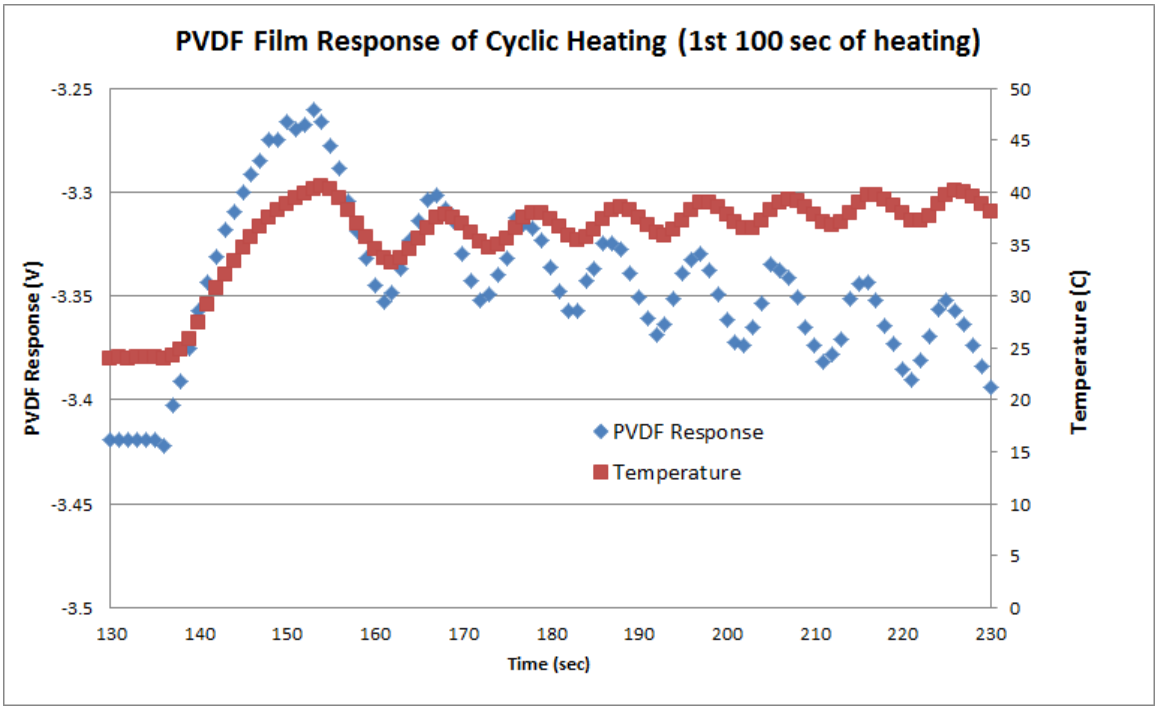

Figure 60. Surface mounted PVDF film initial response to heating

However, since the overall heating profile is not a dynamic event, it is not well described by the response of the PVDF film. As the rate of temperature change levels off, the response of the PVDF film tends back to its null value as shown in Figure 61.

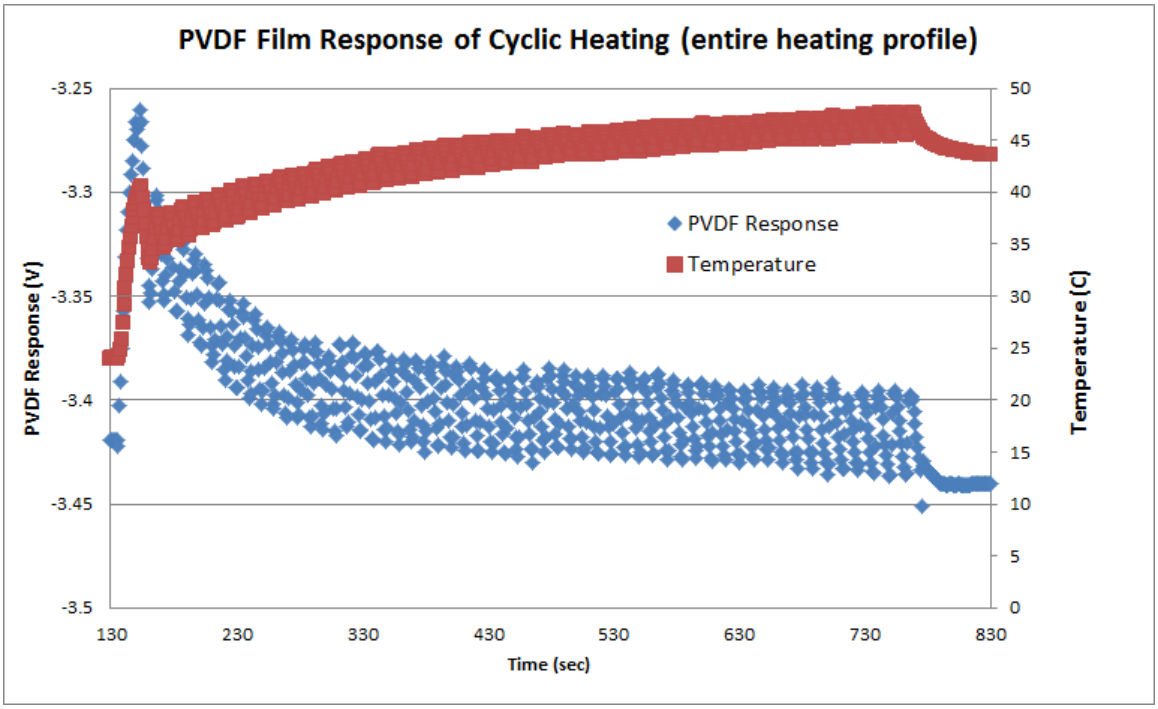

Figure 61. Surface mounted PVDF film extended response to heating

Finally, to ensure that the effects of heating the PVDF film could be canceled out, the modified charge amplifier circuit shown in Figure 22 was tested. By effectively canceling out an identical signal in the sensors, the thermal response can be canceled out. By utilizing one of the sensors as a dummy gage (non-loaded sample), only the mechanical loads will be registered. During heating, the single gage configuration responds well to the oscillatory nature of the oven, whereas the dual gage configuration shows little to no response to the heating as illustrated in Figure 62. It was noted that the gages were very sensitive to location in the oven. If one of the gages of the dual configuration was closer to the heating element, the effects would not be completely canceled out since there was a temperature difference between the two gages.

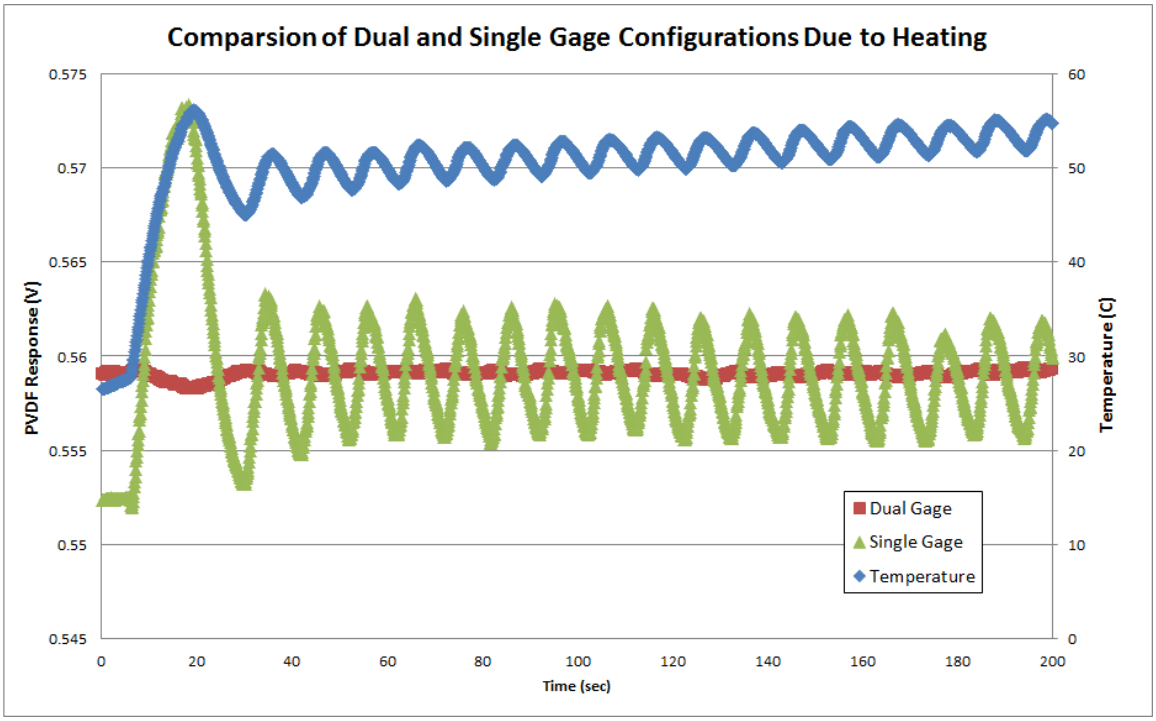

Figure 62. A test of the dual configuration gage to show that ability to eliminate thermal stimuli

From the previous results, no combined loading conditions were performed, as the response from either heating or mechanical loading would begin to return to its null value.

Protocol for Health Monitoring

As has been shown through the results, it is possible to separate out the mechanical and thermal strains with reasonable accuracy, so it is possible to utilize the gages for health monitoring of wind turbine blades, as well as the in-situ cure monitoring. One of the simplest measures to put in place is to watch for the MFSG to fail which would be indicated by a short across the circuit. This will indicate that the composite

material has gone past a given yield strength, and should therefore be investigated for critical failure.

Another set of tests could be performed to measure the stiffness of the blade under only gravitational loading while the turbine is shut off. This measurement could be measured over time, and the decrement in stiffness over the lifetime of the blade could be analyzed to determine when the blade needs to be replaced. Due to the changing strains in the material from varying wind conditions and changing rotational effects, identifying any issues with the blade are strongly dependent on the sampling rate. With a very quick sampling rate, the rotational speed of the blade could be measured by measuring the time between maximum or minimum strains as this would likely occur as the blade is straight up or down. With this quick of a sample rate, a first ply failure may show up as a quick jump in the maximum strain.

The PVDF films showed the ability to sense transient events, and measure the rate of the event. This leads to these sensors being well adapted for measuring weather intensity such as rain or hail hitting the blade. They could also be used for acoustic emission monitoring which detects the noise produced from failure of the composite material.

CONCLUSIONS & FUTURE WORK

Conclusions

The objective of this research project was to manufacture glass fiber composite samples with embedded sensors, and analyze the response of the gages.

- Manufacturing
    - Several iterations of the manufacturing process were done in order to ensure that human induced errors were minimized
    - Different methods for removing the lead wires with minimal disturbance to the surrounding fiber tows and simplicity were investigated
- Literature reviews on the various sensors along with the circuits used to measure their response were performed and a test plan was formed from the information found
- Due to the unpredictable environmental changes in the field, it was imperative to be able to separate the mechanical and thermal strains registered by the gages, so several circuits were designed and tested to validate the assumptions made.
- Metal foil strain gage testing
    - The MFSGs showed the most promise in being implemented in a system for structural health monitoring
    - A 3-wire MFSG is required for accurately measuring any thermal conditions, as any change in temperature of the lead wires for the 2-wire QB will skew the results

  - When compared to the extensometer, the 3-wire MFSG showed an average error of 0.8% indicating that they are accurately describing the response of the sample
  - The sensitivity of the gages was found to be -2.030 ± 6.4% με/(μV/V) for mechanical loading and -0.543 ± 11.75% °C/(μV/V) for thermal loading
  - To calibrate the sensor to any configuration of gage and layup, a combined loading test should be performed with an extensometer and thermocouple, and the sensitivities can be calculated from data obtained

- PVDF film testing
  - Due to the dynamic nature of the PVDF films, they are good at sensing transient events
  - As they always tend to their equilibrium value, they are not well suited for measuring the decay in mechanical properties of the material as it ages or steady state loads
- For both types of sensors, three gages are needed to be able to measure the thermal and mechanical strains
  - One gage is set up to be effected by both thermal and mechanical loading (QB and single gage configuration)
  - Two gages are needed in the other circuit, where one of the gages is used as a dummy gage that will cancel out the thermal loads (HB and dual gage configuration)

- Fiber Optics
    - A literature review of the various types of fiber optics was performed
        - Spatial resolution of 1 cm up to 70 meters along a single fiber along with accuracy of ±1 μstrain and ± 0.1 °C has been demonstrated
    - It was determined that further research should be conducted utilizing these sensors
- Test Matrix comparison
    - Each phase of the test matrix was followed and after each step was found satisfactory, the next test could be performed
    - The experiments performed as expected, and the principal goal of separating the mechanical and thermal strains was achieved
- To calibrate any strain gage, along with any matrix/fiber combination, a simple heating and tensile test should be performed
    - The measured voltage from the tensile test can be compared to an external extensometer to calculate the sensitivity
    - The measured voltage from the thermal test can be compared to a thermocouple response to calculate the thermal sensitivity
- Applications of work
    - The sensors embedded can be used to measure mechanical and thermal strains of composite materials

- Protocol for embedding sensors has been developed and can be followed for other sensors
- Can embed other sensors and use a similar calibration process for measuring the sensitivity of the sensor to the different stimuli
- Provides enough information to allow for repeatable results and minimize the time required for learning how to take accurate measurements

Future Work

As all of the testing has been performed using uni-directional composites, and pure tensile testing, there are many more experiments required to fully characterize the sensors. A list of suggestions for future work is shown below.

- Vary the fiber orientation to better imitate the layups typically found in wind turbine blade manufacturing
- Flexure and mixed mode testing to illustrate the loads seen in typical operation
- Fatigue testing to ensure the ability of the gages to be used for long-term monitoring of the blades
- Test samples to failure to characterize how the gages respond to different failure modes
- Acoustic emission monitoring using the PVDF films
- Design and use of an environmental chamber to accurately control and manipulate the temperature of the sample while undergoing various loading conditions
- Revisit the fiber optic research

    - Use FBG and polarization maintaining fiber optics to measure temperature and strain
    - Investigate surface treatment for these sensors
    - Utilize non-coated fibers for cure monitoring
- Validation in full scale blades
    - Embed sensors in sub-structure and full scale components of wind turbine blades
        - The same manufacturing procedure should be followed except that the lead wires should run through the length of the structure
        - Compare the strength of the material when weaving the lead wires through the tows of the material to extracting them entirely along the length of the structure
    - Determine criteria for unsafe operating conditions of wind turbine blade
        - Maximum strain allowed, stiffness degradation, maximum strain rate
        - Critical locations need to be located for implementation of gages
        - Develop program to indicate critical value reached
- This will allow blades to be inspected/replaced before catastrophic failure, with fewer inspection intervals than currently required

- Limitations of sensors
    - Due to the exposed metal on the MFSGs, these sensors would need to be coated if used with carbon fiber, a carbon infused matrix, or any electrically conductive combination

REFERENCES CITED

[1] E. J. Barbero, *Introduction to Composite Materials Design*. 2011.

[2] D. W. Workshop and G. W. Power, "An Overview of Composite Wind An Overview of Composite Wind Turbine Blade Manufacturing by References sites used in preparing this presentation h," 2010.

[3] J. Thomas, "New Record: World's Largest Wind Turbine (7+ Megawatts)," 2008. .

[4] "Go Go Gadget: Robotic Crawler Rides Up 300-Foot Poles to Inspect Wind Turbine Blades." [Online]. Available: http://www.gereports.com/go-go-gadget/. [Accessed: 13-Jun-2012].

[5] J. F. Manwell, J. G. McGowan, and A. L. Rogers, *Wind Energy Explained*. Wiley, 2003.

[6] S. Manfred, "Wind Turbines 2.1," vol. 2, pp. 11-27, 2008.

[7] "The Lily Dutch Windmill." [Online]. Available: http://www.waratahsoftware.com.au/pages/postcards/wp_thelily_pa210118.html.

[8] "Judith Gap Wind Farm." [Online]. Available: http://dnrc.mt.gov/Trust/Wind/JudithGap.asp.

[9] "Gurit - Blade Structure." [Online]. Available: http://www.gurit.com/files/documents/3_blade_structure.pdf.

[10] "OCS Alternative Energy and Alternate USe Programmatic EIS." [Online]. Available: http://ocsenergy.anl.gov/guide/wind/. [Accessed: 04-Jun-2012].

[11] "Dogger Bank Offshore Wind Farm EIA." [Online]. Available: http://www.royalhaskoning.co.uk/en-gb/fields/industryandenergy/Energy/Pages/dogger-bank-offshore-wind-farm.aspx. [Accessed: 04-Jun-2012].

[12] "Wind Turbine Blade Manufacturing Plant." [Online]. Available: http://www.wind-turbine-blade.net/tag/wind-turbine-blade-manufacturing-plant/.

[13] "Sensor Definition." [Online]. Available: http://www.merriam-webster.com/medical/sensor.

[14] J. C. Blockey, “Feasibility in Developing Smart Structures for Use in Wind Turbine Blades,” no. July, 2008.

[15] N. Palmer, “Smart Composites: Evaluation of Embedded Sensors in Composite Mateirals,” 2009.

[16] “Omega Pre-Wired Strain Gages.” [Online]. Available: http://www.omega.com/pptst/Prewired_GP_Strain_KFG.html. [Accessed: 31-May-2012].

[17] A. Wheeler and A. Ganji, *Introduction to Engineering Experimentation*, 2nd ed. Upper Saddle River, New Jersey: Pearson Education, Inc.

[18] A. Hambley, *Electrical Engineering - Principles and Applications*, Fourth. 2008.

[19] “National Instruments - Strain Gauge Measurement.” [Online]. Available: http://www.eidactics.com/Downloads/Refs-Methods/NI_Strain_Gauge_tutorial.pdf. [Accessed: 01-Jun-2012].

[20] a. Ajovalasit, “Advances in Strain Gauge Measurement on Composite Materials,” *Strain*, vol. 47, no. 4, pp. 313-325, Aug. 2011.

[21] M. E. Tuttle and H. F. Brinson, “Resistance-foil strain-gage technology as applied to composite materials,” *Experimental Mechanics*, vol. 24, no. 1, pp. 54-65, Mar. 1984.

[22] H. F. Castro, S. Lanceros-Méndez, and J. G. Rocha, “Separation of the Pyro- and Piezoelectric Response of Electroactive Polymers for Sensor Applications,” *Materials Science Forum*, vol. 514–516, pp. 202-206, 2006.

[23] F.-K. Chang, *Health Monitoring 2005 - Advancements and Challenges for Implementation*. 2005.

[24] “Seebeck effect,” *Encyclopaedia Britannica*. .

[25] “Omega Temperature.” [Online]. Available: http://www.omega.com/temperature/z/pdf/z021-032.pdf.

[26] “Luna Technologies - Fiber Optic Products.”

[27] “Timbercon - Microbending.” [Online]. Available: http://www.timbercon.com/Microbending.html.

[28] D. A. Hare and T. C. Moore, “Characteristics of Extrinsic Fabry-Perot Interferometric (EFPI) Fiber-Optic Strain Gages,” *Office*, no. December, 2000.

[29] L. Jin and G. Kai, “An embedded FBG sensor for simultaneous measurement of stress and temperature,” *IEEE Photonics Technology Letters*, vol. 18, no. 1, pp. 154-156, Jan. 2006.

[30] S. W. James, M. L. Dockney, and R. P. Tatam, “Simultaneous independent temperature and strain measurement using in-fibre Bragg grating sensors,” *Electronics Letters*, vol. 32, no. 12, pp. 1133-1134, 1996.

[31] W.-chong Du, X.-ming Tao, and H.-yaw Tam, “Fiber Bragg grating cavity sensor for simultaneous measurement of strain and temperature,” *IEEE Photonics Technology Letters*, vol. 11, no. 1, pp. 105-107, 1999.

[32] H.-K. Kang, D.-H. Kang, C.-S. Hong, and C.-G. Kim, “Simultaneous monitoring of strain and temperature during and after cure of unsymmetric composite laminate using fibre-optic sensors,” *Smart Materials and Structures*, vol. 12, no. 1, pp. 29-35, Feb. 2003.

[33] M. Froggatt, D. Gifford, S. Kreger, M. Wolfe, and B. Soller, “Distributed Strain and Temperature Discrimination in Unaltered Polarization Maintaining Fiber.”

[34] D. K. Gifford, B. J. Soller, M. S. Wolfe, and M. E. Froggatt, “Distributed Fiber-Optic Temperature Sensing using Rayleigh Backscatter,” no. 1, pp. 2-3, 2000.